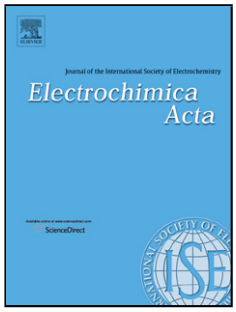

Title: Spectroelectrochemistry of alternating ambipolar copolymers of 4,4′- and 2,2′-bipyridine isomers and quaterthiophene

Authors: Pawel Zassowski, Sylwia Golba, Lukasz Skorka, Grazyna Szafraniec-Gorol, Marek Matussek, Dawid Zych, Witold Danikiewicz, Stanislaw Krompiec, Mieczyslaw Lapkowski, Aneta Slodek, Wojciech Domagala

PII: S0013-4686(17)30076-2
DOI: http://dx.doi.org/doi:10.1016/j.electacta.2017.01.076
Reference: EA 28743

To appear in: *Electrochimica Acta*

Received date: 20-10-2016
Revised date: 11-1-2017
Accepted date: 12-1-2017

Please cite this article as: Pawel Zassowski, Sylwia Golba, Lukasz Skorka, Grazyna Szafraniec-Gorol, Marek Matussek, Dawid Zych, Witold Danikiewicz, Stanislaw Krompiec, Mieczyslaw Lapkowski, Aneta Slodek, Wojciech Domagala, Spectroelectrochemistry of alternating ambipolar copolymers of 4,4′- and 2,2′-bipyridine isomers and quaterthiophene, Electrochimica Acta http://dx.doi.org/10.1016/j.electacta.2017.01.076

Highlights

- New 4,4'-bipyridine derivatives C-substituted with bithiophene groups were prepared.
- Their polymerisation afforded novel polymers with 4,4'bipyridine and viologen groups in the main chain.
- Conjugation disruption in 4,4'-bipyridine copolymers stabilises doping induced polarons.
- 4,4'-bipyridine copolymer chain topology promotes intermolecular π-π interactions.
- The viologen repeating unit copolymer demonstrates strong charge trapping/detrapping effects.

Graphical Abstract

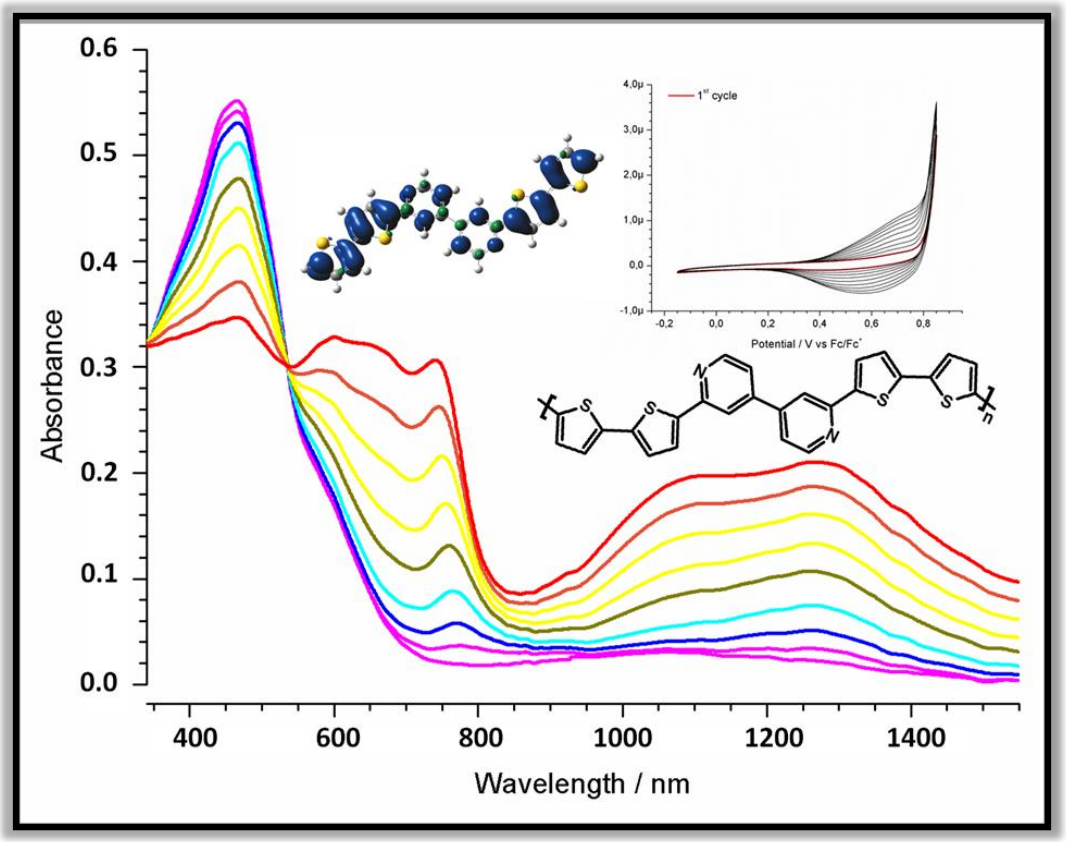

Spectroelectrochemistry of alternating ambipolar copolymers of 4,4'- and 2,2'-bipyridine isomers and quaterthiophene

Pawel Zassowski[a], Sylwia Golba[b], Lukasz Skorka[c], Grazyna Szafraniec-Gorol[d], Marek Matussek[d], Dawid Zych[d], Witold Danikiewicz[e], Stanislaw Krompiec[d], Mieczyslaw Lapkowski[a,f], Aneta Slodek[d*], Wojciech Domagala[a*]

[a] Department of Physical Chemistry and Technology of Polymers, Silesian University of Technology, M. Strzody 9, 44-100 Gliwice, Poland,

[b] Institute of Materials Science, University of Silesia, 75 Pulku Piechoty, 1A, 41-500 Chorzow, Poland

[c] Faculty of Chemistry, Warsaw University of Technology, Nowakowskiego 3, 00-664 Warsaw, Poland

[d] Institute of Chemistry, Faculty of Mathematics, Physics and Chemistry, University of Silesia, Szkolna 9, 40-007 Katowice, Poland,

[e] Polish Academy of Science, Institute of Organic Chemistry, Kasprzaka 44/52, PO box 58, 01-224 Warsaw 42, Poland

[f] Centre of Polymer and Carbon Materials, Polish Academy of Sciences, M. Curie-Sklodowskiej 34, 41-819 Zabrze, Poland

*Corresponding authors.

E-mail addresses: aneta.slodek@us.edu.pl, a.slodek@wp.pl (A. Slodek)

wojciech.domagala@polsl.pl (W. Domagala)

Abstract

First report of π-conjugated push-pull copolymer systems with 4,4'-bipyridine moieties in the main macromolecular chain is presented. C-substitution pattern of electropolymerisable bithiophene pendants at the 4,4'-bipyridine unit offered the versatility to retain the latter as free amine, or convert it into bipyridylium salt. Both structures have been prepared and investigated, delivering the first example of a polymer with viologen unit making up the extended π-bond. Detailed electrochemical, spectroelectrochemical and quantum chemical study of these new polymer systems and their 2,2'-bipyridine analogues has shown that while linear structure and extended conjugation in the latter help it to accommodate charge carriers characteristic for heavily doped polythiophene, the conjugation break afforded by the meta substitution pattern across the 4,4'-pirydyl unit makes the polymer behave like an ensemble of shorter oligomeric segments with better defined electron transitions and sharper and faster electrochromic response. Effective π-π interchain coupling between α,ω-bis(2-pyridyl)quaterthiophene repeating units was observed, whereas intramolecular interactions were found to dominate in the linear 2,2'-bipyridyl based polymer. While the bithiophene derivative of methyl viologen electropolymerised less easily than its corresponding non-quaternised derivative, the resulting polymer films demonstrated decent stability when subject to subsequent p- and n-doping, featuring pronounced charge trapping/detrapping signatures. Furthermore, ion pairing between the viologen and weakly basic PF_6^- and $CF_3SO_3^-$ counterions has been found to impact the redox chemistry of bithiophene functionalised viologen structure. Experimental findings have been confronted with results of quantum chemical computations helping to elucidate the electrochemical and spectroelectrochemical observations made. Presented study delivers insights into the doping processes taking place in

conjugation disrupted 4,4'-bipyridine core copolymers, helping to evaluate their potential as substrates for new tuneable π-conjugated polymeric systems.

Keywords

Conjugated polymer; bipyridine; viologen, thiophene; push-pull systems; polaron; bipolaron;

1. Introduction

Oligo- and polythiophene molecules are playing an important role in the field of organic electronics, on account of their advantageous electronic and optical properties [1,2]. In order to tailor their properties for specific applications, functionalization is an effective means to achieve this goal [3]. Depending on the desired effect, thiophenes can be coupled with either electron deficient or electron rich π-conjugated units to craft the electronic structure of the resulting target. This molecular donor-acceptor engineering concept has received enormous attention in the last decade owing to its numerous successes in the field of organic electronics. Among conceivably countless possibilities of matching different π-conjugated units, the bipyridine moiety has long been in the scope of interest. Of three different symmetric isomers of this double heterocyclic unit: 2,2'-bipyridine, 3,3'-bipyridine and 4,4'-bipyridine, the first has been by far the most intensively researched motif owing to its chelating properties, making it a handy substrate for developing elaborate organic ligand scaffolds. Many derivatives of 2,2'-bipyridine with thienyl [4–11], bithienyl [11–16], and oligothienyl [11] pendants at the 4,4'- [5–7,9,10,13,14] and 5,5'- [4,8,12,14,15] positions have been prepared and described in the literature as ligands in Ru [4–10,13], Zn, or Cu [16] complexes. All these organometallic structures were dedicated to organic electronics, examined primarily for dye-sensitized solar cells technology [5–10,13,15], while free ligands were investigated as polymerisable precursors for conducting polymers and metal-organic hybrid materials [4,12,14,16]. On the other hand, 4,4'-bipyridine is the best known for its N-alkyl quaternary pyridinium salts, dubbed viologens, featuring two reversible redox pairs associated with the stepwise reduction of the bipyridine dication. These redox transitions are marked with distinct and sharp colour changes, and for that reason, viologens have been used as electrochromic materials long before π-conjugated polymers came into play [17]. Being efficient redox mediators, viologens have been also investigated as electrocatalytic [18] and bioelectronic materials [19]. Considering their merits,

numerous conjugated polymers have been functionalized with 4,4'-bipyridinium units as grafted pendants [20–23], preserving the physicochemistry of the viologen unit, affording both electron and redox conductive materials. Curious as it may seem, little work has been done to date on incorporating the quaternised bipyridinium unit into main π-conjugated chain polymer architecture to tap its redox properties, with our group presenting the first report of a 2,2'-bipyridine diquat thiophene copolymer featuring broad visible light absorbing properties with narrow band gap and well defined electrochemistry [12]. On account of different possible substitution patterns of the two pyridine rings, various π-conjugation arrangements within the bipyridine unit, and towards its substituents, can be envisaged. While the enhanced conjugation of the 2,2' and 4,4' isomers stems from the *ortho* and *para* coupling of the pyridine nitrogens, the remaining four available carbon locants afford different degrees of conjugation between the possible π-conjugated substituents. Of the two sterically unhindered locant pairs in 2,2'-bipyridine, 5,5' positions are more favourable giving *para* conjugation of the pendants, but at the same time *meta* miscommunication with the nearest nitrogen atom. The 4,4'-bipyridine enjoying accessible nitrogen lone pairs, features only one sterically unobstructed locant set though – the 2,2' one. In this configuration, the substituents readily communicate with the *ortho* positioned pyridine nitrogen, while suffering a conjugation break at the double *meta* pattern across the otherwise well conjugated bipyridine unit. Considering the possibility of tuning the nucleophilic – electrophilic character of the bipyridine unit through quaternisation, yielding promising results as reported previously [12], we decided to prepare and investigate a new group of 4,4'-bipyridine-quaterthiophene copolymers as potential tuneable donor-acceptor π-conjugated macromolecules, and compare them with their 2,2'-bipyridine counterparts. A set of compounds presented in **Scheme 1** will be considered, and their detailed spectroelectrochemical and quantum mechanical analysis elaborated.

2. Experimental

2.1. Syntheses

All syntheses were carried out under argon atmosphere. The NMR spectra were recorded at room temperature on Bruker Avance 400 MHz instrument in $CDCl_3$, DMSO-d_6, and CD_3CN solvents. Melting point measurements were done on Stuart SMP40 automatic melting analyser. HRMS spectra were recorded in methanol on Mariner ESI-TOF (Applied Biosystems) mass spectrometer using polyethylene glycol 400 (PEG 400) sodiated ions as an internal standard. The following compounds were synthesized by the methods described in the literature: 5,5'-bis(2,2'-bithiophen-5-yl)-2,2'-bipyridine (**2**) [12]; 3,10-bis(2,2'-bithiophene-5-yl)-6,7-dihydropyrido[1,2-a:2',1'-c]pyrazinodiynium hexafluorophosphate (**2a(PF$_6$)$_2$**) [14]; 4,4'-bipyridine-N,N'-dioxide (**A**) [24] and 2,2'-bithiophene-5-boronic acid (**C**) [25].

*2.1.1. Synthesis of bipyridine derivative **1**, and its methyl viologen salts **1a(OTf)$_2$**, and **1a(PF$_6$)$_2$***

2,2'-Bis(2,2'-bithiophen-5-yl)-4,4'-bipyridine (**1**), unreported to date, has been synthesized according to the method presented in **Scheme 2**. Compound **A** has been described in the literature and was synthesized by us with the aid of procedure described in [26]. Compound **B** is also known [27], but we prepared it according to the method reported by Szulc and co-workers [24] for 5,5'-dichloro-2,2'-bipyridine. Fortunately, this procedure turned out to be effective for the synthesis of **B**. Substrate **C**, *i.e.* 2,2'-bithiophene-5-boronic acid has been also described in the literature and was obtained by us according to the procedure outlined in [25]. Finally, we obtained 2,2'-bis(2,2'-bithiophen-5-yl)-4,4'-bipyridine (**1**) *via* coupling **B** with **C**, in a manner similar to that reported for coupling 2,2'-bithiophene-5-boronic acid with

dibromothiophene derivatives [28]. It is worth mentioning, that dichlorobipyridine turned out to be sufficiently reactive and coupling towards **1** proceeded successfully. Compound **1** was converted to bis(bithiophenyl)methylviologen (**1a**) ditriflate (**1a(OTf)$_2$**), and bis(hexafluorophosphate) (**1a(PF$_6$)$_2$**) salts. 1,1'-Dimethyl-2,2'-bis(2,2'-bithiophen-5-yl)-4,4'-bipyridinium bis(triflate) (**1a(OTf)$_2$**) was obtained as a dark orange solid by addition of 10 equivalents of methyl trifluoromethanesulfonate to solution of **1**. Counterion exchange for PF_6^- was performed by treatment of **1a(OTf)$_2$** with the solution of ammonium hexafluorophosphate in methanol (**Scheme 3**).

2.1.2. Synthesis of bipyridine derivatives

Synthesis of **2,2'-dichloro-4,4'-bipyridine (B)**. Phosphorous oxychloride $POCl_3$ (18.65 ml, 0.2 mol) was added to 4,4'-bipyridine-N,N'-dioxide (**A**) (1.88 g, 10.0 mmol) and the solution was refluxed for 3 hours. The reaction mixture was poured onto crushed ice and then neutralized with saturated solution of K_2CO_3 to give a bright green precipitate. The crude product was filtered off, washed with acetone and dried under vacuum (1.78 g, 79% yield). The structure of the product was confirmed by ^{1}H NMR, ^{13}C NMR and ESI-MS analysis. Without further purification it was used to obtain (**1**).

Synthesis of **2,2'-bis(2,2'-bithiophen-5-yl)-4,4'-bipyridine (1)**. An aqueous solution of Na_2CO_3 (1.0 M, 15.0 ml) was added to a solution of 2,2'-dichloro-4,4'-bipyridine (**B**) (0.21 g, 0.95 mmol), 2,2'-bithiophene-5-boronic acid (**C**) (0.44 g, 2.09 mmol) and $[Pd(PPh_3)_4]$ (0.14 g, 0.12 mmol, 6 mol%) in DME (20 ml). The resulting mixture was refluxed for 48h and then cooled to room temperature yielding a green precipitate. The solid was filtered off and washed with diethyl ether. The crude product was dissolved in a small amount of dichloromethane, then precipitated by addition of diethyl ether. The solid was filtered off and finally washed with diethyl ether to give the target compound **1** as a bright green solid (207

mg, 45% yield). Mp (dec.) 174 °C; ^{1}H NMR (400 MHz, DMSO-d_6) **Fig. S1**: δ 7.14 (dd, J = 5.03 Hz, 3.62 Hz, 2H), 7.42 (d, J = 3.91 Hz, 2H), 7.44 (dd, J = 3.59 Hz, 1.06 Hz, 2H), 7.57 (dd, J = 5.06 Hz, 1.00 Hz, 2H), 7.82 (dd, J = 5.17 Hz, 1.46 Hz, 2H), 8.05 (d, J = 3.90, 2H), 8.46 (s, 2H), 8.69 (d, J = 5.10 Hz, 2H); ^{13}C NMR (100 MHz, $CDCl_3$): δ 116.3, 119.7, 124.3, 124.5, 125.0, 125.8, 128.0, 135.0, 137.2, 140.1, 146.7, 150.3, 153.2.; HRMS(+) calcd for $[C_{26}H_{16}N_2S_4 + H]^+$ 485.0275, found 485.0280.

Synthesis of **1,1'-dimethyl-2,2'-bis(2,2'-bithiophen-5-yl)-4,4'-bipyridinium bis(triflate) (1a(OTf)$_2$)**. 2,2'-Bis(2,2'-bithiophen-5-yl)-4,4'-bipyridine (**1**) (160 mg, 0.33 mmol) was dissolved in 5 ml of $CHCl_3$. The reaction mixture was flushed with argon and stirred for 30 minutes. The mixture was heated to 60 ºC and then methyl trifluoromethanesulfonate (541 mg, 0.36 ml, 3.3 mmol) was slowly injected through the septum. During the addition of methyl trifluoromethanesulfonate, the color of solution started changing to dark orange. The mixture was stirred under reflux for additional 6 hours. After cooling to room temperature, the precipitate was filtered off, washed with small amount of $CHCl_3$, and hexane. The product was dried in vacuum giving 241 mg (90%) of dark orange powder. ^{1}H NMR (400 MHz, CD_3CN) **Fig. S2a**: δ 8.89 (d, J = 6.7 Hz, 2H), 8.53 (s, 2H), 8.32 (d, J = 6.4 Hz, 2H), 7.74 (d, J = 4.0 Hz, 2H), 7.56 (d, J = 5.1 Hz, 2H), 7.52 (dd, J = 8.0, 3.4 Hz, 4H), 7.20 – 7.14 (m, 2H), 4.42 (s, 6H); ^{13}C NMR (101 MHz, CD_3CN) **Fig. S2b**: δ 151.34, 149.84, 148.90, 146.25, 136.92, 135.64, 130.28, 129.80, 129.29, 128.72, 127.41, 125.93, 125.26, 49.05; HRMS(+) calcd. for $[C_{28}H_{22}N_2S_4]^{2+}$ 514.06549, found m/z = 257.0338 ($1a^{2+}$).

Synthesis of **1,1'-dimethyl-2,2'-bis(2,2'-bithiophen-5-yl)-4,4'-bipyridinium bis(hexafluorophosphate) (1a(PF$_6$)$_2$)**. Compound **1a(OTf)$_2$** (150 mg, 0.18 mmol) was heated in 10 ml of MeOH. When **1a(OTf)$_2$** dissolved completely, a solution of ammonium hexafluorophosphate (293 mg, 1.8 mmol) in 3 ml of MeOH was added. A reddish precipitate formed immediately. The product was filtered off, washed with water, MeOH and Et_2O and

dried in vacuum to afford 69 mg (48%) of reddish powder. ^{1}H NMR (400 MHz, CD_3CN) **Fig. S3a**: δ 8.86 (d, J = 6.7 Hz, 2H), 8.51 (s, 2H), 8.29 (d, J = 6.6 Hz, 2H), 7.72 (d, J = 3.9 Hz, 2H), 7.53 (d, J = 4.9 Hz, 2H), 7.49 (dd, J = 7.6, 3.7 Hz, 4H), 7.18 – 7.14 (m, 2H), 4.40 (s, 6H); ^{13}C NMR (101 MHz, CD_3CN) **Fig. S3b**: δ 151.29, 149.81, 148.85, 146.19, 136.87, 135.62, 130.21, 129.76, 129.26, 128.66, 127.37, 125.90, 125.21, 49.00; ^{31}P NMR (162 MHz, DMSO-d_6) **Fig. S4**: δ -131.04, -135.43, -139.82, -144.21, -148.60, s-153.00, -157.59 (septet, $J_{P\text{-}F}$ = 711 Hz); HRMS(+) calcd. for $[C_{28}H_{22}N_2S_4]^{2+}$ 514.06549, found m/z = 257.034 ($1a^{2+}$).

2.2. Electrochemical and spectroelectrochemical experiments

Electrochemical measurements (Cyclic Voltammetry and Differential Pulse Voltammetry) were performed using Metrohm Autolab M101 or PGSTAT 100N potentiostats, with a three electrode setup comprising platinum wire working electrode, platinum wire counter electrode and silver wire quasi-reference electrode; calibrated versus ferrocene/ferrocenium redox couple prior to each experiment. All electrochemical experiments were conducted in 0.1 M basic electrolyte solution of tetrabutylammonium hexafluorophosphate - Bu_4NPF_6 (Aldrich) or tetrabutylammonium trifluoromethanesulphonate - Bu_4NOTf (Fluka) in dichloromethane (Aldrich – Chromasolv HPLC grade) or acetonitrile (Carlo Ebra – HPLC plus grade). Solutions were deaerated with argon prior to experiments with inert atmosphere maintained during measurements. Ionization potentials (IP) and electron affinities (EA) of investigated molecules were determined from their redox potentials using the equations [29]:

$$IP = |e|(E_{onset,ox} + 5.1) \quad \text{(eq.1)}$$

$$EA = -|e|(E_{onset,red} + 5.1) \quad \text{(eq.2)}$$

where: E_{onset} – onset potential of oxidation (for determination of IP) or reduction (for determination of EA) of species, e – charge of an electron.

Polymers were obtained by oxidative electropolymerisation from solutions of respective monomers in the above electrolytes, using cyclic voltammetry. Scan rates of 0.1 V/s and 0.05 V/s were used for preparing polymer films on platinum and ITO (Indium Tin Oxide) coated glass electrodes respectively. After synthesis, polymer films were rinsed with pure solvent in order to remove residual monomer. Electrochromic performance of polymer films was investigated for layers having an active area of 0.7 cm^2 immersed in the same electrolyte medium as used for electropolymerisation. Polymer coated electrodes were placed in a 2mm optical path length QS quartz cuvette (Hellma Analytics) fitted with platinum wire counter electrode and silver wire quasi-reference electrode. Autolab PGSTAT 302N potentiostat combined with modular Ocean Optics QE 65000 and NIRQuest512 diode array spectrometers illuminated by Ocean Optics DH-2000-BAL lamp were used. Considering inherent trade-offs between electrochromic contrast, switching rate and polymer film thickness [30,31] thin polymer films were prepared to maximise their optical response times. Repeatedly charging the polymer films between doped and undoped states, their transmittance at selected wavelengths was monitored. Optical response times (switching times) were recorded for 95% complete transmittance changes. The choice of analytic wavelengths for each polymer followed peak signatures of its spectra in either undoped or doped states. Doping charge densities have been computed by integration of current-time profiles recorded simultaneously during switching experiments, and are uncorrected for capacitive charge. Coloration efficiency (CE) was calculated according to known equation [32].

In situ UV-Vis spectroelectrochemical experiments on reduction of **1a(PF$_6$)$_2$** and **1a(OTf)$_2$** in solution were done in a thin layer spectroelectrochemical cell using ITO glass as a working electrode. Analyte and basic electrolyte concentrations were identical to those used

in electrochemical measurements. Measurements were performed on HP-8543 diode array spectrometer.

In situ EPR spectroelectrochemical experiments on reduction of **1a(PF$_6$)$_2$** and **1a(OTf)$_2$** in solution were performed in a custom made glass cylindrical cell, using platinum wire as a working electrode. Measurements were performed using JEOL JES-FA200 EPR spectrometer, equipped with JEOL ES-MCX3B(E) transmission cavity.

In situ simultaneous EPR/UV-Vis-NIR spectroelectrochemical measurements combined the above spectrometer with Ocean Optics QE 65000 and NIRQuest512 diode array spectrometers for tandem collection of EPR and optical spectra. Ocean Optics DH-2000-BAL lamp was used as a light source. Light was directed to and from the EPR spectrometer cavity using lens terminated optical fibres. Polymer samples were deposited on 0.3 mm thick glass electrodes, covered with ITO layer. Counter and quasi-reference electrodes were the same as those used in electrochemical experiments. Electrochemical doping of polymers was carried in custom made thin (0.5 mm) layer quartz cell, using the same electrolytic solution as in electrochemical experiments. All spectra were recorded in potentiostatic mode. Relative spin concentrations were obtained by double integration of EPR spectra.

2.3. Quantum-chemical computations

Density Functional Theory (DFT) calculations were carried out using Gaussian09 Revision B package [33]. DFT calculations were carried out using hybrid B3LYP [34–36] exchange correlation potential combined with 6-31G(d,p) basis set. Ground-state geometries were fully optimized until a stable local minimum was found, which was confirmed by normal-mode analysis (no imaginary frequencies were present). Initial structures were constrained to the highest possible symmetry point group and then relaxed if a saddle point was found. In order to improve numerical accuracy of calculations two-electron integrals and

their derivatives were calculated in a modified way employing the pruned (99.590) integration grid consisting of 99 radial shells and 590 angular points per shell. The ground-state geometries were then optimized in solution using polarizable continuum model (PCM) [37] at the same level of theory, with dichloromethane as solvent. The oscillator strengths and energies of the vertical singlet excitations were calculated employing time-dependent version (TD) of DFT [38–44] and again at the same level of theory (vide supra) with dichloromethane as the solvent. The TD-DFT results were retrieved from output files using GaussSum 2.2 [45]. Molecular orbital plots were generated from cube files with Gabedit 2.4.6 [46]. Spin densities were plotted with gOpenmol [47].

3. Results and discussion

3.1. Optical and electrochemical properties

3.1.1. Bis(bithiophene) bipyridines

UV-Vis spectra of compounds **1** and **2** are presented in **Fig. 1**, with the relevant spectroscopic data collected in **Table 1**. Both **1** and **2** feature single peak spectra with absorption maxima at 366 and 399 nm for **1** and **2**, respectively. The bathochromic displacement is a first manifestation of differences in electronic properties between **1** and **2** on account of their different bipyridine and bithiophene substitution patterns. Clearly the *para* arrangement of bithiophene arms lowers the energy of the principal electron transition compared to *meta* arrangement in **1**, but 30 nm difference turns out to be in fact half of 65 nm one between absorption maxima of 4,4’-bipyridine (237 nm) [48] and 2,2’-bipyridine (302 nm) [49]. Since both compounds are isomers, this situation must be caused by different degree of conjugation in **1** compared to **2**, resulting in a shift of absorbance maximum. This

reflects the electron coupling pattern, where substitution with bithienyl moieties at the *para* position of 2,2'-bipyridine leads to enhanced conjugation across the whole molecule compared to *meta* substitution at 4,4'-bipyridine unit in **1.**

Electrochemistry of investigated monomers is presented in **Fig. 2**, while the numeric data is collected in **Table 1.** Both **1** and **2** undergo irreversible oxidation, however the onset potential of this process is different. Oxidation of **1** starts at 0.88 V vs. Fc/Fc^+ that is 0.29 V higher than of **2**. In the reverse scan one can observe a reduction current, originating from products of electropolymerisation on the platinum electrode. These will be discussed in detail further on. Reduction of compounds **1** and **2** is also electrochemically irreversible, however, in this case, no electroactive products are detected. Onset potentials of reduction are also different, being 0.13 V more negative for **1**. Oxidation and reduction onsets of investigated compounds have been used for calculation of ionization potential (IP) and electron affinity (EA) values [29], while the difference gave electrochemical frontier energy gap of the molecules (**Table 1**). The data demonstrates that both IP and EA values contribute to higher electrochemical bandgap of **1** compared to **2**, indicating that the latter is better conjugated, in accord with UV-Vis spectra.

Electrochemical oxidation of compounds **1** and **2** yields electroactive films on the surface of the working electrode (**Fig. 3a** and **b**). Electrochemical polymerisation of **1** occurs when potential higher than 0.8 V vs. Fc/Fc^+ is applied, with repetitive cycling resulting in formation of electroactive film covering the surface of the electrode. Electrochemical polymerisation of **2** proceeds in a manner similar to reports of Swager et al. [4] giving electroactive deposit featuring reversible double step redox response between 0.5 and 1.1 V vs. Fc/Fc^+. The fact that both **1** and **2** undergo oxidative polymerisation could be traced to impaired accessibility of lone electron pairs of the pyridines towards reaction with electrophiles like the thiophene radical cation being the precursor of oxidative polymerisation

of C_α unsubstituted thiophenes [50]. Pyridines are known as efficient electrophile scavengers on account of their Lewis base character, but introduction of bulky substituents at their 2 and 5 positions is known to hinder this trait, making pyridines selective nucleophiles depending on the size and chemical nature of these substituents. This property has been recently utilised to prepare electropolymerisable pyridine derivatives of common π-conjugated heterocycles like thiophene [51] where the pyridine nitrogen's lone pair is effectively barred from quenching intermediate radical cations that propagate the polymer chain growth. Important to note here is that compounds **1** and **2** demonstrate that substitution of just one *ortho* position to the pyridine nitrogen atom can be sufficient to make that pyridine derivative open to electropolymerisation.

Cyclic voltammetry of films obtained on platinum electrode is presented in **Fig. 3c** and **3d**. For both **p1** and **p2** oxidation proceeds as a wave, with the onset at 0.27 and 0.06 V vs. Fc/Fc^+, respectively. Similar difference in oxidation potential was also seen for monomers, leading to conclusion that factors responsible for this situation in **1** and **2** are also at play in **p1** and **p2**. This includes already discussed *para* vs. *meta* substitution pattern at the two bipyridine isomers and its influence on coupling between thiophene units. Both polymers can be electrochemically n-doped, however their stability in this state is poor with prolonged cycles of n-doping and dedoping leading to electrode passivation. The onset of reduction is: -2.11 and -2.01 V for **p1** and **p2**, respectively (**Table 2**). These values are lower compared to monomers by ca. 0.15 - 0.20 V indicating increased electron donating effect of quaterthiophenes flanking the bipyridine unit in the polymer. Investigating basic charge transfer kinetics of p-doping process of **p1** and **p2**, one finds that both polymers feature linear scan rate dependence of characteristic anodic and cathodic currents of their CVs (**Fig. S5**) in their whole stable working potential window. Linear dependencies of both anodic and cathodic current signatures indicate that both doping and dedoping processes of the films

operate in the kinetic regime, being not limited by counterion diffusion effects. This in turn suggests that ionic conductivity outperforms apparent electrical conductivity of films of both polymers, which will reverberate in colorimetric switching time experiments discussed below.

Electrodeposited films of **p1** and **p2** change their colour upon p-doping, switching from red in their neutral state to grey and yellow for **p1** and **p2**, respectively. Depositing them at an optically transparent ITO electrode, their electrochromic performance dynamics have be investigated. Switching the polymers between neutral and oxidized states, time-resolved changes of their transmittance have been recorded for three characteristic wavelengths (**Fig. 4**) featuring highest transmittance modulations, and subsequent electrochromic efficiency parameters computed (**Table 3**). Polymer **p1** shows contrast in the range of 9.8 to 20%, with relatively long switching times from 11.1 to 16.7 seconds. Coloration efficiency for this layer was in the range of 116 to 199 $cm^2 \cdot C^{-1}$, with the best value obtained at 741 nm. Compared to **p1**, electrochromic properties of **p2** were inferior. Depending on investigated wavelength, chromic contrast was smaller or similar, with values between 4.0 and 21.2%. Colour change kinetics, however, were distinctively slower, varying from 38.2 to 46.3 seconds, while the coloration efficiency for corresponding wavelengths followed chromic contrast's suit (55.8 to 186.6 $cm^2 \cdot C^{-1}$). Given that charge transfer resistance at the polymer/ITO interface will be higher than at the polymer/Pt one, the established kinetic, rather than diffusive control of charging and discharging of investigated polymers indicates that their electrochromic performance is determined by their sluggish electron transport properties. Stability of colour switching turned also to be an issue, with progressive deterioration of electrochromic properties being observed for both polymers, manifested by lower contrast values in each subsequent doping/dedoping cycle. Such electrochromic device failure has been well documented with oxygen and UV light being principal contributors to photochemical degradation of π-conjugated electrochromes [52].

To investigate redox doping behaviour of **p1** and **p2** in more detail, simultaneous EPR/UV-Vis-NIR spectroelectrochemical experiments have been performed, providing valuable information about the mechanism of electrochemical processes taking place in these polymers [53]. Optical spectra recorded during these experiments are presented in **Fig. 5**, EPR signals in **Fig. 6**, and spin concentration plots are given in **Fig. 7**. Recalling theoretical work [54], two fundamental types of charge carriers can be envisioned during oxidation state charge of a non-degenerate ground state conjugated polymer: polarons (radical cations) and bipolarons (dications). Formation of polaron entails appearance of two new optical transitions, while formation of bipolaron brings about only one new optical transition. Higher energy transition of polaron should be placed in the Vis region, while the lower energy transition in the NIR region. Bipolaron transition should be placed in between two polaron transitions. Products of interaction of these carriers, e.g.: π-dimers, have been also put forward in order to explain some experimental data with their two electron transitions being hypsochromically shifted relative to polaron transitions and the third one usually concealed beyond the low energy resolution edge of UV-Vis-NIR spectrometers [55–57]. Investigated polymers in their neutral state are characterized by fundamental absorption maxima located at 463 and 488 nm for **p1** and **p2**, respectively (**Fig. 5**). These are red-shifted compared to monomers, on account of extended conjugation in polymers afforded by quaterthiophene units formed upon electropolymerisation. A difference of 25 nm in absorption maxima of **p1** and **p2** is similar to that between monomers **1** and **2**, suggesting 2,2'-bipyridine and 4,4'-bipyridine substitution pattern as the anticipated cause. Changes in the optical spectra of **p1** and **p2** take place when potential higher than onset of oxidation is applied. In both polymers, π-π^* transition lowers its intensity, albeit to markedly disparate extent, while two new composite peaks appear and increase in intensity with increasing potential. Maxima of these peaks fall at 670, 770, 1090, and 1270 nm for **p1** and 756 and 1240 nm with higher energy shoulders for **p2**. With

increasing potential, steady and regular change of UV-Vis-NIR spectra is observed suggesting both quantitative and qualitative changes in the population of doping borne charge carriers. Owing to composite nature of observed peaks it is very convenient to analyse the differences between consecutive pairs of spectra (**Fig. S6**). Such comparison helps to trace out trends in changes of optical density at particular wavelengths making it possible to discern possible liaisons between individual spectral bands. Analysing progressive absorbance differences for **p1** it stands clear that the peaks at 770 and 1270 nm are coupled together, just as the 670 and 1090 nm peak pair is. The first pair grows in intensity right from the beginning of doping of **p1** while the second pair follows suit, overtaking the first one at the highest potentials. There is also one additional doping induced band at ca. 570 nm that appears to evolve alongside the two pairs discussed above. For **p2** the situation is different. At the onset of oxidation of this polymer, the first prominent band growth takes place at 800 nm and only above 0.45 V vs. Fc/Fc^+ does another band come into the stage at 1260 nm. Like for **p1**, here as well, a second companion to this peak can be traced out at 750 nm growing synchronously with it. Despite overlap with the 800 nm peak, a second peak pair can be spotted at ca. 680 and 1070 nm. Likewise in **p1**, this second band pair develops as an auxiliary feature of the 750, 1260 nm peak doublet attaining comparable intensity only at the highest doping potential of **p2**.

EPR spectra (**Fig. 6**), recorded simultaneously with above discussed UV-Vis-NIR spectra, offer invaluable complementary information about the doping mechanism in both polymers, allowing to discriminate between the signals of spin bearing (polarons) and spinless (π,σ-dimers, bipolarons) since EPR spectroscopy permits selective observation of spin active species only. Similarly to the optical spectra, in both **p1** and **p2**, one can observe changes in spin concentration (**Fig. 7**) when potential higher than onset of oxidation is applied. For **p1**, spin concentration growth coincides with appearance of NIR doping induced bands indicating polaron formation taking place in this polymer right from the onset of its p-doping. In line

with this observation, the peak pair at 770 and 1270 nm can be assigned to these spin bearing species. In the solid state, intermolecular interactions are an important phenomenon shaping physicochemical properties of investigated thin polymer films. Oligo and polythiophenes are particularly inclined to form associates even in dilute solutions [58], and studies of tailor made double-stacked oligothiophenes [59] have shown that additional electron transitions take place between configuration mixed electron levels of closely interacting pairs of oligothiophene chains. In particular, three electron transitions are predicted and observed in a radical cation of an oligothiophene dimer compared to two, foreseen in an isolated oligothiophene chain. Owing to Davydov shift, transitions in stacked oligothiophene take place at higher energies compared to ones taking place in solitary chains. These facts neatly explain the rearrangements in UV-Vis-NIR spectra taking place in **p1** upon its p-doping. Linear increase of unpaired spins together with potential offset growth of band intensities at 570, 670 and 1090 nm all indicate an equilibrium establishing between polarons loosely and tightly interacting with neighbouring undoped polymer chains. Such interactions have been observed in thin solid oligothiophene films where the first electrochemical oxidation peak was found to involve the transfer of $0.5e^-$ per oligothiophene molecule providing quantitative indicators of formation of stable charged-uncharged oligothiophene dimers [23,60]. Considering the conjugation pattern of bipyridine and quaterthiophene units in **p1**, radical cations are confined to α,ω-bis(pyridyl)quaterthiophene sub-units, which, on account of pyridine's electrophilic character are unlikely to support double cation charge. The zig-zag structure of **p1** though, offers an assortment of possible arrangements of this bent macromolecule, facilitating local overlapping of neighbouring α,ω-bis(pyridyl)quaterthiophenes segments of the polymer chain and creating opportunity for effective interchain coupling. The situation in **p2** is strikingly different in that respect since its substitution pattern favours flat geometry of the polymer chain, as indicated by DFT

optimization of geometry of **p2** and its dimer. Linear structure of this polymer's chain makes the effectiveness of its interchain π-π interactions dependent on the angle between the major axes of two adjacent chains. Considering statistical factors alone of effecting an eclipsing overlap of two linear polymer chains, it appears far less probable for **p2** to adopt a stacked structure with intermolecular π-conjugation between oligothienyl pairs, effectual enough to activate pimer specific electron transitions. This would explain the weak spectral signatures of such associates in the UV-Vis-NIR spectra of doped **p2** and dominance of polaron transitions stabilised at loosely interacting polymer segments. Despite statistically minor population of effectively aligned **p2** macromolecules, their interactions prove strong enough to favour formation of bipolarons at low doping levels [61–64] as evidenced by the shape of UV-Vis-NIR spectra of **p2** and the absence of EPR signal growth in it up to 0.4 V vs. Fc/Fc^{+}. Polymer **p2** enjoys linear structure imparted by *para* substitution across the pyridinium sub-unit where conjugation of a charged specie can proceed freely along the whole length of the macromolecule. Such conditions stabilise higher charged species like bipolarons, making disproportionation of nascent polarons favourable as has been observed in oligothiophene model compounds [65].

Recapitulating the above discussion, experimental data clearly suggests that the thienyl substitution pattern at the bipyridine moiety plays a crucial role in shaping the physicochemistry of the two polymer isomers. While **p2**'s linear structure and extended conjugation help it to accommodate charge carriers characteristic for heavily doped polythiophene [66–68], the conjugation break afforded by the *meta* substitution pattern across the pirydyl unit makes **p1** behave like an ensemble of shorter oligomeric segments with better defined electronic structure. In such setting, 4,4'-bipirydyl tunes the electron energy levels of this thiophene copolymer, an approach effectively demonstrated with other heterocyclic units whose doping behaviour resembles that observed for **p1** [69,70]. Compared to other electron

deficient heterocyclic units, bipyridine's basic character offers auxiliary means to modify its electrophilic character by way of quaternisation of the nitrogen atom's lone electron pair. Viologen derivatives so obtained are well known electrochromophores whose redox features should confer conveniently reversible n-doping ability to this otherwise p-dopable polythiophene copolymer.

3.1.2. Bisbithiopheneviologens

Upon quaternisation of **1**, its bipyridinium salts **1a(PF$_6$)$_2$** and **1a(OTf)$_2$** feature UV-Vis spectra with two absorption maxima (**Fig. 8**), unlike those of both bithiophene and methyl viologen. In **1a^{2+}** ion, the central 4,4'-bipyridinium moiety acts as an electron acceptor, while bithienyl, a known electron-rich unit, functions as an electron donor. Combined together in one molecule, they afford a structure with polarised electron density distribution disclosing a characteristic charge transfer band in the visible region located at 416 and 427 nm for **1a(PF$_6$)$_2$** and **1a(OTf)$_2$**, respectively. Similar, but considerably red-shifted spectral feature was found for **2a(PF$_6$)$_2$** at 530 nm. The nature of this and other electron transitions will be discussed in more detail together with results of DFT calculations. While the principal spectral bands at 335 nm for **1a(PF$_6$)$_2$** and 339 nm for **1a(OTf)$_2$** are displaced by 40 meV, the offset of maxima of charge transfer bands of these ionic isologues amounts to 80 meV suggesting difference in binding energy of ion pair complex of **1a^{2+}** with hexafluorophosphate and trifluoromethanesulfonate anions. This is curious considering both anions are equally valent and negligibly basic, and the solvent (acetonitrile) should be polar enough to effectively shield the opposite ions from direct electrostatic interactions. Despite high dielectric constant, however, the donicity (donor number) of acetonitrile is only moderate [71], meaning that its solvating ability towards the **1a^{2+}** cation may be insufficient to afford an effective separation of the viologen – counterion pair [72]. As concerns anions, solvent

dielectric constant and the free energy of anion solvation are uncorrelated [71], with acetonitrile demonstrating limited solvation ability of anions on account of its moderate donor number. Counterion influence, particularly on the electrochemical properties of viologen redox reactions, has been observed for different inorganic and organic anions in various solvents [17] and $\mathbf{1a}^{+2}$ turns out to be sensitive to this subtle cation-anion interplay as the results of the following experiments disclose.

Transformation of **1** and **2** into their bipyridinium salts modifies their electrochemical properties (**Fig. 9** and **Table 4**). Unexpectedly, the onset of oxidation in $\mathbf{1a(PF_6)_2}$ and $\mathbf{1a(OTf)_2}$ is shifted negative by ca. 0.1 V, while for $\mathbf{2a(PF_6)_2}$ a change of 0.3 V in the positive direction is recorded. Likewise for **1** and **2**, oxidation of $\mathbf{1a(PF_6)_2}$, $\mathbf{1a(OTf)_2}$, and $\mathbf{2a(PF_6)_2}$ is irreversible and results in electroactive film deposition. In the range of negative potentials, $\mathbf{1a(PF_6)_2}$, $\mathbf{1a(OTf)_2}$, and $\mathbf{2a(PF_6)_2}$ demonstrate two step reduction process characteristic for viologens [17] and diquats [73]. The course of the redox reactions turns out to be strongly counterion dependent and **Fig. 9** shows remarkably different voltammograms of reduction of the viologen unit in $\mathbf{1a(PF_6)_2}$ compared to $\mathbf{1a(OTf)_2}$. Viologens undergo two, single electron reduction steps, transforming them first into a radical monocation, and then into electroneutral bis(1,4-dihydropyridine) derivative. When all redox species are soluble in the electrolyte medium and diffusion limited electron transfer conditions prevail at the surface of the electrode, a cyclic voltammogram with two separated and well defined redox pairs is observed. Such is the case for $\mathbf{1a(PF_6)_2}$, where two identical, reversible peak signals are seen and the DPV trace with two equal height peaks suggests that both steps involve the same number of electrons. Change of counterion has a significant impact on the shape of CV of $\mathbf{1a(OTf)_2}$ where distinctively dissimilar peak currents are observed in both cathodic and anodic segments and the DPV trace hints that the number of electrons involved in the second redox step is double that of the first step. Approximation of background corrected peak

current intensities at each redox step yields ratios of $^{2}i_c/^{1}i_c$ of ca. 1 and 2 for **1a(PF$_6$)$_2$** and **1a(OTf)$_2$** respectively with the sum of peak currents at each step ($^{1}i_c + {}^{2}i_c$) being comparable for both salts. Aberration of this peak current ratio has been observed for viologen functionalised polymers [74] where the reduction steps take place in the solid state. Counterion was found to influence viologen's reduction reaction but this effect again involved precipitation of insoluble electroreduction products [75,76]. The regularities observed for **1a(PF$_6$)$_2$** and **1a(OTf)$_2$** are baffling as all species are soluble, and the sum of currents of both reduction steps appear independent of the vologen's counterion. Considering that CV responses show these reactions to be at least chemically reversible, the issue must rest in some effect common to all four (two reduction and two reoxidation) redox steps considered. It could well be that acetonitrile's weakness in establishing diffusion double layer around the individual ions of investigated salts and their electron transfer products may be the underlying cause of dissimilarities of observed redox properties of **1a(PF$_6$)$_2$** and **1a(OTf)$_2$** with both salts existing as ion pairs in their common anion electrolyte solutions employed.

Thin film spectroelectrochemistry is a convenient tool to investigate reversible redox processes under exhaustive electrolysis conditions. In order to probe the phenomena of reduction of **1a^{+2}** ion in different ionic environments, spectroelectrochemical observation of **1a(PF$_6$)$_2$** and **1a(OTf)$_2$** reduction was done. After the compounds are reduced to their radical cation state (at -0.75 V), their optical spectra (**Fig. 10a** and **b**) evidence changes including blue-shift of charge transfer (CT) transition to a value of ca. 395 nm for both molecules and simultaneous growth of radical cation band at ca. 650 nm tailing to near-infrared region. This band is characteristic for viologen radical monocations [77,78] and it is worth noting here that no clear signs of π-dimer bands, expected around 550 nm and above 800 nm, are seen [79–81] indicating that either **1a(PF$_6$)** and **1a(OTf)** radical cations do not dimerise or dimerise negligibly. Further reduction to neutral state brings further changes in the optical spectra of

the two salts. Stepping the potential to -1.15 V, the radical cation band vanishes, while new transition forms around 500 nm. Single electron reduction of $\mathbf{1a}^{+\bullet}$ radical cation yields electroneutral **1a** molecule hence spectra of doubly reduced **1a(PF$_6$)** and **1a(OTf)** should be similar. This is the case though only qualitatively since band maxima of **1a** in PF_6^- electrolyte are hypsochromically displaced compared to OTf^- electrolyte. Considering both $\mathbf{1a}^{+2}$ and **1a** differ by two electrons, the pattern of their electron transitions should be similar, which is indeed the case. Apparent differences in shape and spectral band positions manifest charge transfer character of **1a** responding to different ionic environment this molecule is generated in.

EPR spectroelectrochemical experiments conducted on **1a(PF$_6$)$_2$** and **1a(OTf)$_2$** confirm that their first cathodic step generates radical cations [17,79]. Their EPR signals are strong (**Fig. 10c** and **d**) featuring complex hyperfine structure, similar to spectra of different viologen radical cation derivatives [82–85]. Analysis of these counterion-specific hyperfine patterns allowed to elaborate on unpaired spin distribution in radical cations of **1a(PF$_6$)** and **1a(OTf)**. Spectra of both radical ions could be successfully simulated using a set of hyperfine coupling constants listed in **Fig. S7**. Spin density calculations indicate that despite *ortho* arrangement relative to each nitrogen atom where the spin density is the highest, unpaired electron hardly delocalises onto bithienyl units, supporting the assignment of hyperfine coupling constants made. Individual coupling constants differ between **1a(PF$_6$)** and **1a(OTf)** suggesting individual coulombic interactions between $\mathbf{1a}^{+\bullet}$ and the two different counterions. The fundamental spectral linewidth is found to be the same for both radical cation salts, but EPR line shape turns out to be a different combination of Gauss and Lorentz components. This suggests different spin relaxation dynamics of the unpaired electron in **1a(PF$_6$)** and **1a(OTf)**, which is probably a reflection of differences in ion pair binding energies of investigated radical cation salts. This inkling aligns with findings presented above, indicating

both thermodynamic and kinetic factors of ion pairing equilibria could be responsible for the disparity of redox behaviour of **1a(PF$_6$)$_2$** and **1a(OTf)$_2$** and their reduction products [86,87].

Electrochemical polymerisation of **1a(PF$_6$)$_2$** and **1a(OTf)$_2$** (**Fig. 11a** and **b**) proceeds differently compared to **1**. Cyclic potential sweep results in new small peak visible at 0.6 V; shifting its position to higher potential in each subsequent cycle. Similar behaviour was also observed for **2a(PF$_6$)$_2$** [12]. Oxidation of **1a(PF$_6$)$_2$** and **1a(OTf)$_2$**, just like **2a(PF$_6$)$_2$** effectively affords trication radical whose third positive charge is confined to the bithienyl segment. Coupling of such highly charged bithiophene radical cations is hindered by their poor stability, resulting in inferior electropolymerisation efficiency. In the case of **2a(PF$_6$)$_2$**, this problem was overcome by adding 10% of $BF_3{\cdot}Et_2O$ to electropolymerisation solution; leading to decrease of oxidation potential of the monomer. Boron trifluoride assisted electropolymerisation resulted in deposition of an electroactive **p[2a(PF$_6$)$_2$]** layer, which did not shift its peak potential from cycle to cycle. This approach failed for **1a(PF$_6$)$_2$** and **1a(OTf)$_2$**, however. We also attempted to electropolymerise **1a(PF$_6$)$_2$** and **1a(OTf)$_2$** on the surface of ITO electrodes for spectroelectrochemical measurements (described below), but the layers obtained were electroinactive.

The electrochemistry of **p[1a(PF$_6$)$_2$]** and **p[1a(OTf)$_2$]** is different, compared to both **p1** and **p[2a(PF$_6$)$_2$]** (**Fig. 11c** and **d**). Oxidation onset of polymer layers falls at 0.60 and 0.55 V (**Table 5** and **Fig. S8**) for **p[1a(PF$_6$)$_2$]** and **p[1a(OTf)$_2$]** respectively, being lower by ca. 0.2 V compared to **1a(PF$_6$)$_2$** and **1a(OTf)$_2$** monomer. Both polymers demonstrate a narrow, ca. 0.2 V range of electroactivity under p-doping conditions. Furthermore, **p[1a(OTf)$_2$]** film turned out to be quickly losing its electroactivity under potential cycling conditions. Reduction onsets (**Table 5** and **Fig. S8**) are very similar to those of monomers, being equal to -0.60 and -0.71 V for **p[1a(PF$_6$)$_2$]** and **p[1a(OTf)$_2$]** accordingly. Similar reduction onsets are expected on account of electropolymerisation unaltered viologen unit

present in both polymers. However, the shape of these voltammograms is distorted compared to those of **1a(PF$_6$)$_2$** and **1a(OTf)$_2$**, particularly for the first reduction step redox pair. On top of that, different voltammogram is obtained when oxidation and reduction cycles follow one another. Both first reduction and oxidation peaks are noticeably sharper since detrapping [88] of p- and n-doping charges takes place, overlapping with CV peaks of p- or n-doped polymers only. When both polymers are doped across both p- and n- doping regimes, very stable electrochemistry is observed with negligible decrease in electroactivity after 50 cycles.

3.2 Quantum-chemical computations

The DFT calculations were carried out on the B3LYP/6-31G(d,p) level of theory. Firstly, the ground-state geometries of **1** and **2** were examined in search of the converged, optimized geometry within a certain point group. For both compounds several initial arrangements were taken into account either within C_{2h} or C_{2v} symmetry point group. However, what was found was that each of these highly symmetric point groups afford a higher-order saddle point. Therefore, the geometries were relaxed and constrained to C_2 point group. At this point it was found, that there are two possible geometries for both **1** and **2**, which are close to the aforementioned C_{2v} or C_{2h}. The results of this study are presented in **Table S1**.

As can be seen, there is a slight difference between values calculated in either geometries for both compounds. However, the E_g value of **1** is higher than that of **2** by about 0.3 eV. This effect is due to the conformational twist about C(4)-C(4) bond in 4,4'-bipyridine core, which deteriorates the overlap of the orbitals and rises the energy gap.

The comparison of frontier molecular orbital energies also gives the idea that the values for **1** and **2** are comparable, with some minor differences though. The HOMO for **1** is 0.2 eV smaller than for **2** (C_{2h} vacuum), while the difference in LUMO is 0.1 eV. On

numerous occasions the simple HOMO/LUMO analysis proved sufficient for oligothiophene derivatives, but it is not always the case. Therefore, the calculations of ionization potentials as the positive difference in energy between the oxidized and the neutral forms in their optimized geometries were also carried out. The solvation effects were implemented with the PCM model and dichloromethane as solvent. In many cases the IP value does not simply correspond to the HOMO level of a given molecule due to the dynamic background of the former. It is therefore more reliable to compare these parameters with their experimental values. In the case of **1** and **2**, the vacuum IP values deviate by almost 1.0 eV, making them unreliable. However, when solvation is taken into account the IPs decrease making almost a perfect match with HOMO levels of **1** and **2**.

On the one hand, the comparison of the DFT data with the experimental results reveals satisfactory correlation of HOMO (IP) values with cyclic voltammetry data. Literature reports provide abundant examples of high consistency of B3LYP results with experimental data for polythiophene species [89]. On the other hand though, the LUMO values are underestimated by ca. 0.8 eV. This can be attributed to the fact that simple HOMO/LUMO characteristics of organic semiconductors deals with a static situation, which is insufficient for fine description of electrochemical results. For visualization of the abovementioned data, the plots of HOMOs and LUMOs of **1** and **2** (in one geometry) are presented in **Fig. 12**. As can be seen, LUMOs present similar behaviour for both **1** and **2**, while for **2** the HOMO is more delocalized than for **1**. The difference in the HOMO shape can be attributed to the conformational twist in **1** about C(4)-C(4') in bipyridine moiety making it more localized on the terminal bithiophenes.

We have also simulated the shape and energy of model molecule $\mathbf{1a}^{2+}$ (without the counterion), representative for compounds $\mathbf{1a(PF_6)_2}$ and $\mathbf{1a(OTf)_2}$ (**Fig. 13** and **Table S1**. Contrary to uncharged **1** and **2**, strong localization of frontier orbitals is seen, similarly to the case of $\mathbf{2a}^{2+}$ [12], with occupied orbitals located at bithiophene moieties and LUMO orbitals

located in the centre of the molecule. Methylation of bipyridine also influences the energy of these orbitals lowering both HOMO (-6.12 eV) and LUMO (-3.62 eV), and resulting in a lower E_g (2.50 eV) compared to **1**. Similar relations were observed for bipyridine derivatives and its methylated analogues in electrochemical experiments (**Table 1** and **Table 4**).

In p-doping regime, one could expect similarities in conformational behaviour with oligothiophene systems. In the neutral state, the dihedral angle between thiophene units is of a few degrees. The cation radical species are likely to form more planar conformations, what has been observed for other organic semiconductors [90]. For the studied molecules this phenomenon may also be observed, however for $\mathbf{1}^{+\bullet}$ the planarization occurs for thiophene rings but not for the central bipyridine unit. At these geometries, the spin density plots were generated in order to localize the active site during doping. The plots are presented in **Fig. 14**. It is seen that the spin density is localized mainly on bithiophene moieties in $\mathbf{1}^{+\bullet}$ while being almost evenly distributed throughout $\mathbf{2}^{+\bullet}$ radical cation. These differences clearly indicate the influence of the *meta*- (for $\mathbf{1}^{+\bullet}$) and *para*- (for $\mathbf{2}^{+\bullet}$) substitution pattern of bithienyls at the bipyridine core. Different spin distribution is observed in $\mathbf{1a}^{+\bullet}$. In this case, the majority of unpaired spin is located at the centre bipyridinium unit, spreading only to a small extent onto bithiophene moieties (**Fig. 15**). This explains the stable and repetitive CV curve recorded during reduction of this cation. These results are also consistent with EPR spectroelectrochemical measurements (**Fig. 10**) where stable and intense EPR spectra of $\mathbf{1a}^{+\bullet}$ were recorded.

The electronic spectra for **1** and **2** in the UV-Vis region consist of one intense band, which was simulated using TD-DFT approach (**Fig. S9**). For these calculations, optimized geometries in solution were used taking into account the different possible conformations of studied species. The indicators of the most important vertical excitations are listed in **Table S2**. Analysis of the transitions for **2** is much simpler due to the fact that there is a very tiny

difference between two possible conformations. Therefore, the corresponding band in its UV-Vis spectrum comes predominantly from the HOMO-LUMO transition, which is allowed in this case and highly privileged (**Fig. S9 c** and **d**). This transition is attributed to a mixed excitation from bithiophene moieties to bipyridine and an excitations on bithiophene itself. The second transition is located exclusively on bithiophene. The case of **1** is more complicated due to greater differences between conformation close to C_{2h} and C_{2v} symmetry point group. Judging from **Fig. S9 a** and **b**, the second (close to C_{2v}) conformation provides a better correlation between theory and experiment because the oscillator strength plots almost exactly match the progression of the curve. On the other hand, qualitative analysis of the orbitals involved in transitions brings us to the conclusion that these transitions are very similar. It can be also distinguished that the HOMO-LUMO transition is allowed in one geometry but almost forbidden in the other. Careful analysis reveals, however, that there is another transition close in energy and nature to the HOMO-LUMO excitation (HOMO-1 to LUMO). These excitations contribute to the transition between bithiophene moiety and bipyridine core, and are similar to the analogous case of **2**. For this reason, the composition of transitions in both molecules are almost exactly the same.

More complex spectrum has been obtained for $\mathbf{1a}^{2+}$ (**Fig. S10** and **Table S3**). First two excitations are located at 581 and 557 nm, consisting mainly of transitions from bithiophene to bipyridine moiety. These are probably seen in experimental spectrum wavelengths of 427 nm for $\mathbf{1a(OTf)_2}$ and 416 nm for $\mathbf{1a(PF_6)_2}$ (**Fig. 8** and **Table 1**), confirming their charge transfer character postulated earlier. Two next excitations (simulated wavelengths of 407 and 401 nm) consist of transitions from bithiophene to both bithiophene and bipyridine moieties, similarly to transitions seen in simulated spectrum of **1** and **2**.

The behaviour of polymeric species of **1** and **2** can be analysed on models constructed from two such molecules. In **Fig. 16** the spin density plot for the $\mathbf{1}_2^{+\bullet}$ dimer suggests an

almost exclusive localization of it on the quaterthiophene linkage especially in the central part. This result justifies our interpretation of spectroelectrochemical p-doping experiments of **p1** and **p2** involving generation of positively charged oxidation products on isolated α,ω-bis(pyridyl)quaterthiophene polymer chain segments.

4. Conclusions

Novel 4,4'-bipyridine derivative **1** substituted with bithiophene groups was synthesised and its push-pull characteristics studied and compared to the 2,2'-bipyridine counterpart **2**. Alkyl quaternisation afforded bis(bithiophnene) substituted viologen derivatives **1a(PF$_6$)$_2$** and **1a(OTf)$_2$** which were investigated likewise. Electrochemical polymerisation of the free amine (**1**) and its bipyridylium salts (**1a(PF$_6$)$_2$** and **1a(OTf)$_2$)** afforded new quatertiophene copolymers with 4,4'-bipyridine and viologen units in the main polymer chain, unreported to date.

Substitution pattern of bithiophene groups in isomers **1** and **2** impacts the spectroscopic and electrochemical properties of the two structures, with the degree of conjugation being the primary reason. Compound **1** is characterized by higher band gap (2.84 eV) than **2** (2.42 eV), pointing out improved conjugation in **2** also observed in the UV-Vis spectra. Both compounds undergo electrochemical polymerisation giving insoluble electroactive polymer films **p1** and **p2**. Meta conjugation pattern of quaterthiophenes across the 4,4'-bipyridine unit in **p1** favours formation of polarons which are restricted to α,ω-bis(pyridyl)quaterthiophene repeating units, while the extended conjugation in **p2** chain supports formation of bipolarons. The zig-zag structure of **p1** provides the opportunity for effective interchain π-π coupling of polymer chains, whereas linear structure of **p2** hinders these, promoting intrachain interactions instead. Quantum chemical DFT/TDDFT calculations, performed for two different point groups (C_{2h} and C_{2v}) afforded close correlation

of theoretical predictions with experimental results enabling mechanistic description of the electron transitions taking place to be made.

On account of the ionic nature of the bipyridinium salt entity, viologens **1a(PF$_6$)$_2$** and **1a(OTf)$_2$**, and diquat **2a(PF$_6$)$_2$** demonstrated disparate set of spectroscopic and electrochemical properties compared to their non-quaternised precursors. As expected, viologens **1a(PF$_6$)$_2$** and **1a(OTf)$_2$** undergo two single-electron reduction steps. The reduction to radical cation generates a blue-shifted UV-Vis transition at approx. 390 nm with simultaneous growth of a radical cation band at around 650 nm, characteristic for viologen radical monocation. Final reduction of both salts to neutral state (**1a**) produces a new transition around 500 nm. Cross-correlation of electrochemical and spectroelectrochemical results; the differences in shape and spectral band positions of the two viologens in particular, pointed out the sensitivity of **1a**$^{2+}$ and **1a**$^{+}$ to different ionic environments. Electrochemistry of viologen bearing polymers **p1a(PF$_6$)$_2$** and **p1a(OTf)$_2$** features sharp first reduction and oxidation peaks, ascribable to abrupt release of trapped p- and n-doping charges. These phenomena overlap with CV peaks of p- and n- doping of the polymers, only when both doping regimes are pursued one after another, and it is then that both **p1a(PF$_6$)$_2$** and **p1a(OTf)$_2$** polymers demonstrate stable electrochemical response with negligible decrease in electroactivity.

Presented study delivers insights into the doping processes taking place in conjugation disrupted 4,4'-bipyridine core copolymers, helping to evaluate their potential as substrates for developing new tuneable π-conjugated polymeric systems.

Acknowledgements

Financial support of the Ministry of Science and Higher Education of Poland, awarded through grant no. N N507 326936 is gratefully acknowledged.

This work was supported by the National Centre for Research and Development grant no. PBS2/A5/40/2014.

Gaussian09 calculations were carried out at the Wroclaw Centre for Networking and Supercomputing, WCSS, Wroclaw, Poland. http://www.wcss.wroc.pl, under computational grant no. 18.

References

[1] P. Bujak, I. Kulszewicz-Bajer, M. Zagorska, V. Maurel, I. Wielgus, A. Pron, Polymers for electronics and spintronics, Chem. Soc. Rev. 42 (2013) 8895. doi:10.1039/c3cs60257e.

[2] A. Pron, P. Gawrys, M. Zagorska, D. Djurado, R. Demadrille, Electroactive materials for organic electronics: preparation strategies, structural aspects and characterization techniques, Chem. Soc. Rev. 39 (2010) 2577. doi:10.1039/b907999h.

[3] T. Otsubo, Y. Aso, K. Takimiya, Functional oligothiophenes as advanced molecular electronic materials, J. Mater. Chem. 12 (2002) 2565–2575. doi:10.1039/b203780g.

[4] S.S. Zhu, T.M. Swager, Design of conducting redox polymers: A polythiophene-Ru(bipy)n+ Hybrid Material, Adv. Mater. 8 (1996) 497–500. doi:10.1002/adma.19960080609.

[5] L.E. Polander, A. Yella, B.F.E. Curchod, N. Ashari Astani, J. Teuscher, R. Scopelliti, et al., Towards Compatibility between Ruthenium Sensitizers and Cobalt Electrolytes in Dye-Sensitized Solar Cells, Angew. Chemie Int. Ed. 52 (2013) 8731–8735. doi:10.1002/anie.201304608.

[6] A. Mishra, N. Pootrakulchote, M.K.R. Fischer, C. Klein, M.K. Nazeeruddin, S.M. Zakeeruddin, et al., Design and synthesis of a novel anchoring ligand for highly efficient thin film dye-sensitized solar cells, Chem. Commun. (2009) 7146. doi:10.1039/b912506j.

[7] P.G. Bomben, J. Borau-Garcia, C.P. Berlinguette, Three is not a crowd: efficient sensitization of TiO2 by a bulky trichromic trisheteroleptic cycloruthenated dye, Chem. Commun. 48 (2012) 5599. doi:10.1039/c2cc00136e.

[8] F.-R. Dai, W.-J. Wu, Q.-W. Wang, H. Tian, W.-Y. Wong, Heteroleptic ruthenium complexes containing uncommon 5,5'-disubstituted-2,2'-bipyridine chromophores for dye-sensitized solar cells., Dalton Trans. 40 (2011) 2314–2323. doi:10.1039/c0dt01043j.

[9] F. Gao, Y. Wang, D. Shi, J. Zhang, M. Wang, X. Jing, et al., Enhance the Optical Absorptivity of Nanocrystalline TiO 2 Film with High Molar Extinction Coefficient Ruthenium Sensitizers for High Performance Dye-Sensitized Solar Cells, J. Am. Chem. Soc. 130 (2008) 10720–10728. doi:10.1021/ja801942j.

[10] P.G. Bomben, T.J. Gordon, E. Schott, C.P. Berlinguette, A Trisheteroleptic Cyclometalated RuII Sensitizer that Enables High Power Output in a Dye-Sensitized Solar Cell, Angew. Chemie Int. Ed. 50 (2011) 10682–10685. doi:10.1002/anie.201104275.

[11] G.R. Pabst, O.C. Pfüller, J. Sauer, The new and simple "LEGO" system: Synthesis and reactions of thienyl-substituted 4-tributylstannyl-2,6-oligopyridines, Tetrahedron. 55 (1999) 5047–5066. doi:10.1016/S0040-4020(99)00178-7.

[12] M. Krompiec, I. Grudzka, M. Filapek, L. Skórka, S. Krompiec, M. Lapkowski, et al., An electrochromic diquat-quaterthiophene alternating copolymer: A polythiophene with a viologen-like moiety in the main chain, Electrochim. Acta. 56 (2011) 8108–8114. doi:10.1016/j.electacta.2011.05.132.

[13] J.-Y. Li, C.-Y. Chen, J.-G. Chen, C.-J. Tan, K.-M. Lee, S.-J. Wu, et al., Heteroleptic ruthenium antenna-dye for high-voltage dye-sensitized solar cells, J. Mater. Chem. 20 (2010) 7158. doi:10.1039/c0jm01418d.

[14] S.S. Zhu, R.P. Kingsborough, T.M. Swager, Conducting redox polymers: investigations of polythiophene-Ru(bpy)3n+ hybrid materials, J. Mater. Chem. 9 (1999) 2123–2131. doi:10.1039/a903193f.

[15] C.-Y. Chen, S.-J. Wu, C.-G. Wu, J.-G. Chen, K.-C. Ho, A Ruthenium Complex with Superhigh Light-Harvesting Capacity for Dye-Sensitized Solar Cells, Angew. Chemie Int. Ed. 45 (2006) 5822–5825. doi:10.1002/anie.200601463.

[16] S.S. Zhu, T.M. Swager, Conducting Polymetallorotaxanes: Metal Ion Mediated Enhancements in Conductivity and Charge Localization, J. Am. Chem. Soc. 119 (1997) 12568–12577. doi:10.1021/ja972794w.

[17] C.L. Bird, A.T. Kuhn, Electrochemistry of the viologens, Chem. Soc. Rev. 10 (1981) 49. doi:10.1039/cs9811000049.

[18] D.R. Wheeler, J. Nichols, D. Hansen, M. Andrus, S. Choi, G.D. Watt, Viologen Catalysts for a Direct Carbohydrate Fuel Cell, J. Electrochem. Soc. 156 (2009) B1201.

doi:10.1149/1.3183815.

[19] J.-H. Kim, W.-C. Park, S.-H. Kim, Immobilized Polyviologen as an Effective Redox Mediator for Microbial Fuel Cells, Bull. Korean Chem. Soc. 32 (2011) 3849–3850. doi:10.5012/bkcs.2011.32.11.3849.

[20] H.C. Ko, S. Park, W. Paik, H. Lee, Electrochemistry and electrochromism of the polythiophene derivative with viologen pendant, Synth. Met. 132 (2002) 15–20. doi:10.1016/S0379-6779(02)00217-5.

[21] H. Cho Ko, J. Yom, B. Moon, H. Lee, Electrochemistry and electrochromism of a poly(cyclopentadithiophene) derivative with a viologen pendant, Electrochim. Acta. 48 (2003) 4127–4135. doi:10.1016/S0013-4686(03)00580-2.

[22] H.C. Ko, M. Kang, B. Moon, H. Lee, Enhancement of Electrochromic Contrast of Poly(3,4-Ethylenedioxythiophene) by Incorporating a Pendant Viologen, Adv. Mater. 16 (2004) 1712–1716. doi:10.1002/adma.200400218.

[23] A. Czardybon, J. Zak, M. Lapkowski, Synthesis, electrochemical and spectroelectrochemical properties of viologen derivative of PEDOT, Pol. J. Chem. 78 (2004) 1533–1541. http://www.scopus.com/scopus/inward/record.url?eid=2-s2.0-6344239059&partner=40&rel=R4.0.0.

[24] J. Mlochowski, Z. Szulc, M. Fikus, A. D. Inglot, Synthesis of Potential Interferon Inducers and DNA Intercalators. Part I. Derivatives of 1,8-Diazafluorene — The Novel Analogues of Tilorone, Heterocycles. 22 (1984) 73. doi:10.3987/R-1984-01-0073.

[25] S. Dufresne, G.S. Hanan, W.G. Skene, Preparation, Photophysics, and Electrochemistry of Segmented Comonomers Consisting of Thiophene and Pyrimidine Units: New Monomers for Hybrid Copolymers, J. Phys. Chem. B. 111 (2007) 11407–11418. doi:10.1021/jp075259j.

[26] D. Wang, W.E. Crowe, R.M. Strongin, M. Sibrian-Vazquez, Exploring the pH dependence of viologen reduction by alpha-carbon radicals derived from HCy and Cys., Chem. Commun. (2009) 1876–1878. doi:10.1039/b819746f.

[27] G.T.M.T. P. Ackermann, D. Stierli, M. Diggelmann, F. E. M. Cederbaum, J-F. Wenger, N-phenyl-[(4-pyridyl)-azinyl]-amine derivatives as plant protection agents, 2007.

[28] D.S. Kim, H.A. Kyo, Fluorescence "turn-on" sensing of carboxylate anions with oligothiophene-based o-(carboxamido)trifluoroacetophenones, J. Org. Chem. 73 (2008) 6831–6834. doi:10.1021/jo801178y.

[29] C.M. Cardona, W. Li, A.E. Kaifer, D. Stockdale, G.C. Bazan, Electrochemical Considerations for Determining Absolute Frontier Orbital Energy Levels of Conjugated Polymers for Solar Cell Applications, Adv. Mater. 23 (2011) 2367–2371. doi:10.1002/adma.201004554.

[30] W.T. Neo, Z. Shi, C.M. Cho, S.-J. Chua, J. Xu, Effects of Chemical Composition, Film Thickness, and Morphology on the Electrochromic Properties of Donor-Acceptor Conjugated Copolymers Based on Diketopyrrolopyrrole, Chempluschem. 80 (2015) 1298–1305. doi:10.1002/cplu.201500182.

[31] T. Jarosz, A. Brzeczek, K. Walczak, M. Lapkowski, W. Domagala, Multielectrochromism of redox states of thin electropolymerised films of poly(3-dodecylpyrrole) involving a black coloured state, Electrochim. Acta. 137 (2014) 595–601.

[32] P.M. Beaujuge, J.R. Reynolds, Color Control in π-Conjugated Organic Polymers for Use in Electrochromic Devices, Chem. Rev. 110 (2010) 268–320. doi:10.1021/cr900129a.

[33] M.J. Frisch, G.W. Trucks, H.B. Schlegel, G.E. Scuseria, M.A. Robb, J.R. Cheeseman, et al., Gaussian, (2009).

[34] C. Lee, W. Yang, R.G. Parr, Development of the Colle-Salvetti correlation-energy formula into a functional of the electron density, Phys. Rev. B. 37 (1988) 785–789. doi:10.1103/PhysRevB.37.785.

[35] A.D. Becke, A new mixing of Hartree–Fock and local density-functional theories, J. Chem. Phys. 98 (1993) 1372. doi:10.1063/1.464304.

[36] A. Becke, Density Functional Thermochemistry III The Role of Exact Exchange, J. Chem. Phys. 98 (1993) 5648–5652. doi:10.1063/1.464913.

[37] J. Tomasi, B. Mennucci, R. Cammi, Quantum Mechanical Continuum Solvation Models, Chem. Rev. 105 (2005) 2999–3094. doi:10.1021/cr9904009.

[38] R. Bauernschmitt, R. Ahlrichs, Treatment of electronic excitations within the adiabatic approximation of time dependent density functional theory, Chem. Phys. Lett. 256 (1996) 454–464. doi:10.1016/0009-2614(96)00440-X.

[39] M.E. Casida, C. Jamorski, K.C. Casida, D.R. Salahub, Molecular excitation energies to high-lying bound states from time-dependentdensity- functionalresponsetheory: Characterizationand correctionofthetime-dependentlocal densityapproximation ionization threshold Mark, J. Chem. Phys. 108 (1998) 4439. doi:10.1063/1.475855.

[40] R.E. Stratmann, G.E. Scuseria, M.J. Frisch, An efficient implementation of time-dependent density-functional theory for the calculation of excitation energies of large molecules, J. Chem. Phys. 109 (1998) 8218. doi:10.1063/1.477483.

[41] C. Van Caillie, R.D. Amos, Geometric derivatives of excitation energies using SCF and DFT, Chem. Phys. Lett. 308 (1999) 249–255. doi:10.1016/S0009-2614(99)00646-6.

[42] C. Van Caillie, R.D. Amos, Geometric derivatives of density functional theory excitation energies using gradient-corrected functionals, Chem. Phys. Lett. 317 (2000) 159–164. doi:10.1016/S0009-2614(99)01346-9.

[43] F. Furche, R. Ahlrichs, Adiabatic time-dependent density functional methods for excited state properties, J. Chem. Phys. 117 (2002) 7433. doi:10.1063/1.1508368.

[44] G. Scalmani, M.J. Frisch, B. Mennucci, J. Tomasi, R. Cammi, V. Barone, Geometries and properties of excited states in the gas phase and in solution: Theory and application of a time-dependent density functional theory polarizable continuum model, J. Chem. Phys. 124 (2006) 94107. doi:10.1063/1.2173258.

[45] N.M. O'boyle, A.L. Tenderholt, K.M. Langner, cclib: A library for package-independent computational chemistry algorithms, J. Comput. Chem. 29 (2008) 839–845. doi:10.1002/jcc.20823.

[46] A.R. Allouche, Gabedita - A graphical user interface for computational chemistry softwares, J. Comput. Chem. 32 (2011) 174–182. doi:10.1002/jcc.21600.

[47] D.L. Bergman, L. Laaksonen, A. Laaksonen, Visualization of solvation structures in liquid mixtures, J. Mol. Graph. Model. 15 (1997) 301–306. doi:10.1016/S1093-3263(98)00003-5.

[48] B.D. Coleman, R.M. Fuoss, Quaternization Kinetics. I. Some Pyridine Derivatives in Tetramethylene Sulfone *, J. Am. Chem. Soc. 77 (1955) 5472–5476. doi:10.1021/ja01626a006.

[49] A. Bartecki, J. Szoke, G. Varsanyi, M. Vizesy, Absorption spectra in the ultraviolet and visible region. Volume 2, Academic Press Inc., New York, 1961.

[50] Y. Li, K. Kamata, T. Kawai, J. Abe, T. Iyoda, Electrochemical synthesis of a pyridinium-conjugated assembly based on nucleophilic substitution of oligothiophene π-radical cation, J. Chem. Soc. Perkin Trans. 1. (2002) 1135–1140. doi:10.1039/b200738j.

[51] P. Pander, P. Data, R. Turczyn, M. Lapkowski, A. Swist, J. Soloducho, et al., Synthesis and characterization of chalcogenophene-based monomers with pyridine acceptor unit, Electrochim. Acta. 210 (2016) 773–782. doi:10.1016/j.electacta.2016.05.185.

[52] J. Jensen, M. V. Madsen, F.C. Krebs, Photochemical stability of electrochromic polymers and devices, J. Mater. Chem. C. 1 (2013) 4826. doi:10.1039/c3tc30751d.

[53] L. Dunsch, Recent Advances in in situ multi-spectroelectrochemistry, J. Solid State Electrochem. 15 (2011) 1631–1646. doi:10.1007/s10008-011-1453-1.

[54] W.R. Salaneck, R.H. Friend, J.L. Brédas, Electronic structure of conjugated polymers: consequences of electron–lattice coupling, Phys. Rep. 319 (1999) 231–251. doi:10.1016/S0370-1573(99)00052-6.

[55] J. Cornil, J.-L. Bredas, Nature of the optical transitions in charged oligothiophenes, Adv. Mater. 7 (1995) 295–297. doi:10.1002/adma.19950070311.

[56] M.G. Hill, K.R. Mann, L.L. Miller, J.-F. Penneau, ChemInform Abstract: Oligothiophene Cation Radical Dimers. An Alternative to Bipolarons in Oxidized Polythiophene.,

ChemInform. 23 (2010) no-no. doi:10.1002/chin.199228151.

[57] A. Smie, J. Heinze, Reversible Dimerization of Diphenylpolyene Radical Cations: An Alternative to the Bipolaron Model, Angew. Chemie Int. Ed. English. 36 (1997) 363–367. doi:10.1002/anie.199703631.

[58] P. Bäuerle, U. Segelbacher, K.-U. Gaudl, D. Huttenlocher, M. Mehring, Didodecylsexithiophene-A Model Compound for the Formation and Characterization of Charge Carriers in Conjugated Chains, Angew. Chemie Int. Ed. English. 32 (1993) 76–78. doi:10.1002/anie.199300761.

[59] K.M. Knoblock, C.J. Silvestri, D.M. Collard, Stacked conjugated oligomers as molecular models to examine interchain interactions in conjugated materials, J. Am. Chem. Soc. 128 (2006) 13680–13681. doi:10.1021/ja063312w.

[60] J. Zak, M. Lapkowski, S. Guillerez, G. Bidan, State of partial oxidation of the regioregular sexi (3-octyl thiophene) oligomer in solid phase on electrode surface, J. Solid State Electrochem. 10 (2006) 134–139. doi:10.1007/s10008-005-0055-1.

[61] M.G. Hill, J.F. Penneau, B. Zinger, K.R. Mann, L.L. Miller, Oligothiophene cation radicals. .pi.-Dimers as alternatives to bipolarons in oxidized polythiophenes, Chem. Mater. 4 (1992) 1106–1113. doi:10.1021/cm00023a032.

[62] R. Takita, C. Song, T.M. Swager, π-Dimer Formation in an Oligothiophene Tweezer Molecule, Org. Lett. 10 (2008) 5003–5005. doi:10.1021/ol8020995.

[63] C. Song, T.M. Swager, π-Dimer Formation as the Driving Force for Calix[4]arene-Based Molecular Actuators, Org. Lett. 10 (2008) 3575–3578. doi:10.1021/ol8013039.

[64] P. Hapiot, P. Audebert, K. Monnier, J.-M. Pernaut, P. Garcia, Electrochemical Evidence of .pi.-Dimerization with Short Thiophene Oligomers, Chem. Mater. 6 (1994) 1549–1555. doi:10.1021/cm00045a012.

[65] P. Frère, M. Allain, E.H. Elandaloussi, E. Levillain, F.-X. Sauvage, A. Riou, et al., Effects of Structural Factors on the π-Dimerization and/or Disproportionation of the Cation Radical of Extended TTF Containing Thiophene-Based π-Conjugated Spacers, Chem. - A Eur. J. 8 (2002) 784–792. doi:10.1002/1521-3765(20020215)8:4<784::AID-CHEM784>3.0.CO;2-U.

[66] M. Trznadel, A. Pron, M. Zagorska, R. Chrzaszcz, J. Pielichowski, Effect of Molecular Weight on Spectroscopic and Spectroelectrochemical Properties of Regioregular Poly(3-hexylthiophene), Macromolecules. 31 (1998) 5051–5058. doi:10.1021/ma970627a.

[67] J. Chen, A.J. Heeger, F. Wudl, Confined soliton pairs (bipolarons) in polythiophene: In-situ magnetic resonance measurements, Solid State Commun. 58 (1986) 251–257. doi:10.1016/0038-1098(86)90212-7.

[68] Y. Harima, T. Eguchi, K. Yamashita, Enhancement of carrier mobilities in poly(3-methylthiophene) by an electrochemical doping, Synth. Met. 95 (1998) 69–74. doi:10.1016/S0379-6779(98)00035-6.

[69] A. Kurowska, A.S. Kostyuchenko, P. Zassowski, L. Skorka, V.L. Yurpalov, A.S. Fisyuk, et al., Symmetrically Disubstituted Bithiophene Derivatives of 1,3,4-Oxadiazole, 1,3,4-Thiadiazole, and 1,2,4-Triazole – Spectroscopic, Electrochemical, and Spectroelectrochemical Properties, J. Phys. Chem. C. 118 (2014) 25176–25189. doi:10.1021/jp507838c.

[70] K. Kotwica, E. Kurach, G. Louarn, A.S. Kostyuchenko, A.S. Fisyuk, M. Zagorska, et al., Alternating copolymers of thiadiazole and quaterthiophenes – Synthesis, electrochemical and spectroelectrochemical characterization, Electrochim. Acta. 111 (2013) 491–498. doi:10.1016/j.electacta.2013.07.209.

[71] U. Mayer, Ionic equilibria in donor solvents, Pure Appl. Chem. 41 (1975) 291–326. doi:10.1351/pac197541030291.

[72] M. Jonsson, A. Houmam, G. Jocys, D.D.M. Wayner, Solvent effects on redox properties of radical ions, J. Chem. Soc. Perkin Trans. 2. 117 (1999) 425–429. doi:10.1039/a809499c.

[73] B.J. Coe, J. Fielden, S.P. Foxon, J.A. Harris, M. Helliwell, B.S. Brunschwig, et al., Diquat Derivatives: Highly Active, Two-Dimensional Nonlinear Optical Chromophores with Potential Redox Switchability, J. Am. Chem. Soc. 132 (2010) 10498–10512. doi:10.1021/ja103289a.

[74] N. Wang, A. Kähkönen, P. Damlin, T. Ääritalo, J. Kankare, C. Kvarnström, Electrochemical synthesis and characterization of branched viologen derivatives, Electrochim. Acta. 154 (2015) 361–369. doi:10.1016/j.electacta.2014.12.075.

[75] R.J. Jasinski, The Electrochemistry of Some n-Heptylviologen Salt Solutions, J. Electrochem. Soc. 124 (1977) 637. doi:10.1149/1.2133376.

[76] S.A. John, H. Kasahara, T. Okajima, K. Tokuda, T. Ohsaka, Electrochemical study on monomer/dimer equilibria of a series of asymmetric viologen monolayers on the electrode surface in the presence of hexafluorophosphate ion, J. Electroanal. Chem. 436 (1997) 267–270. doi:10.1016/S0022-0728(97)00364-1.

[77] C. Lee, M.S. Moon, J.W. Park, Spectroelectrochemical study on monomer/dimer equilibria of methylalkylviologen cation radicals with and without α-cyclodextrin, J. Electroanal. Chem. 407 (1996) 161–167. doi:10.1016/0022-0728(95)04472-8.

[78] R.J. Mortimer, T.S. Varley, In situ spectroelectrochemistry and colour measurement of a complementary electrochromic device based on surface-confined Prussian blue and aqueous solution-phase methyl viologen, Sol. Energy Mater. Sol. Cells. 99 (2012) 213–220. doi:10.1016/j.solmat.2011.11.052.

[79] E.M. Kosower, J.L. Cotter, Stable Free Radicals. II. The Reduction of 1-Methyl-4-cyanopyridinium Ion to Methylviologen Cation Radical, J. Am. Chem. Soc. 86 (1964) 5524–5527. doi:10.1021/ja01078a026.

[80] W. Geuder, S. Hünig, A. Suchy, Single and double bridged viologenes and intramolecular pimerization of their cation radicals, Tetrahedron. 42 (1986) 1665–1677. doi:10.1016/S0040-4020(01)87583-9.

[81] R. Kannappan, C. Bucher, E. Saint-Aman, J.-C. Moutet, A. Milet, M. Oltean, et al., Viologen-based redox-switchable anion-binding receptors, New J. Chem. 34 (2010) 1373. doi:10.1039/b9nj00757a.

[82] G. Grampp, B.Y. Mladenova, D.R. Kattnig, S. Landgraf, ESR and ENDOR investigations of the degenerate electron exchange reactions of various viologens in solution. Solvent dynamical effects, Appl. Magn. Reson. 30 (2006) 145–164. doi:10.1007/BF03166715.

[83] C.S. Johnson, H.S. Gutowsky, High-Resolution ESR Spectra of Photochemically Generated Free Radicals: The Viologens, J. Chem. Phys. 39 (1963) 58. doi:10.1063/1.1734033.

[84] C. Kong, L. Qin, J. Liu, X. Zhong, L. Zhu, Y.-T. Long, Determination of dissolved oxygen based on photoinduced electron transfer from quantum dots to methyl viologen, Anal. Methods. 2 (2010) 1056. doi:10.1039/c0ay00201a.

[85] R.D. Webster, R.A.W. Dryfe, J.C. Eklund, C.-W. Lee, R.G. Compton, In situ electrochemical ESR studies of reactive radicals: the reductions of bromo-anthraquinone and methyl viologen, J. Electroanal. Chem. 402 (1996) 167–174. doi:10.1016/0022-0728(95)04351-9.

[86] P.M.S. Monk, N.M. Hodgkinson, Charge-transfer complexes of the viologens: effects of complexation and the rate of electron transfer to methyl viologen, Electrochim. Acta. 43 (1998) 245–255. doi:10.1016/S0013-4686(97)00091-1.

[87] P.M.S. Monk, N.M. Hodgkinson, R.D. Partridge, The colours of charge-transfer complexes of methyl viologen: effects of donor, ionic strength and solvent, Dye. Pigment. 43 (1999) 241–251. doi:10.1016/S0143-7208(99)00063-7.

[88] R. Borjas, D.A. Buttry, EQCM studies of film growth, redox cycling, and charge trapping of n-doped and p-doped poly(thiophene), Chem. Mater. 3 (1991) 872–878. doi:10.1021/cm00017a024.

[89] S.S. Zade, M. Bendikov, From Oligomers to Polymer: Convergence in the HOMO−LUMO Gaps of Conjugated Oligomers, Org. Lett. 8 (2006) 5243–5246. doi:10.1021/ol062030y.

[90] M. Grucela-Zajac, M. Filapek, L. Skorka, J. Gasiorowski, E.D. Glowacki, H. Neugebauer, et al., Thermal, optical, electrochemical, and electrochromic characteristics of novel polyimides bearing the Acridine Yellow moiety, Mater. Chem. Phys. 137 (2012) 221–234. doi:10.1016/j.matchemphys.2012.09.011.

Schemes

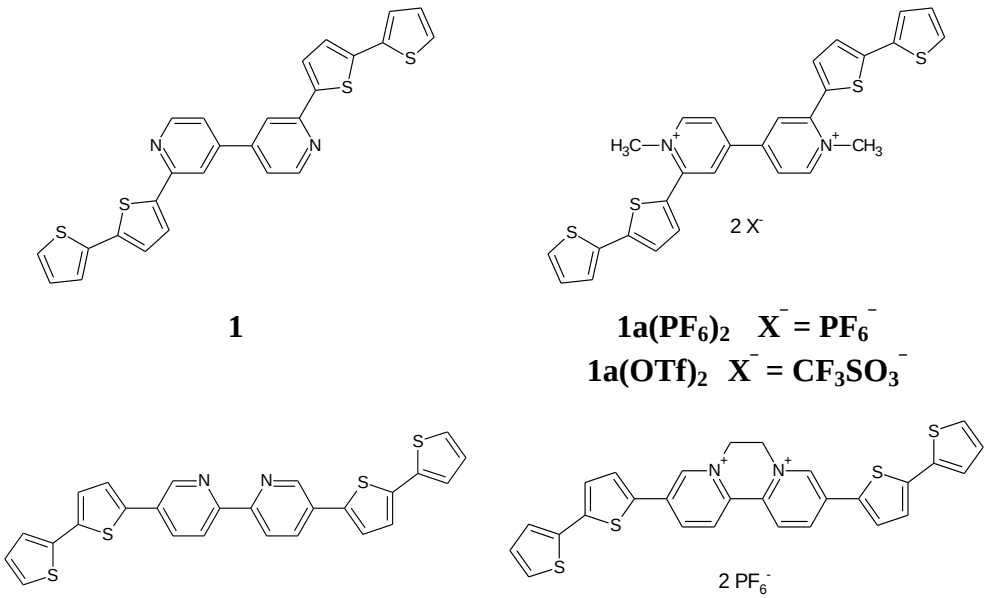

1 **1a(PF$_6$)$_2$ X$^-$ = PF$_6^-$**
1a(OTf)$_2$ X$^-$ = CF$_3$SO$_3^-$

2 **2a(PF$_6$)$_2$**

Scheme 1. Structures of molecules discussed in this work.

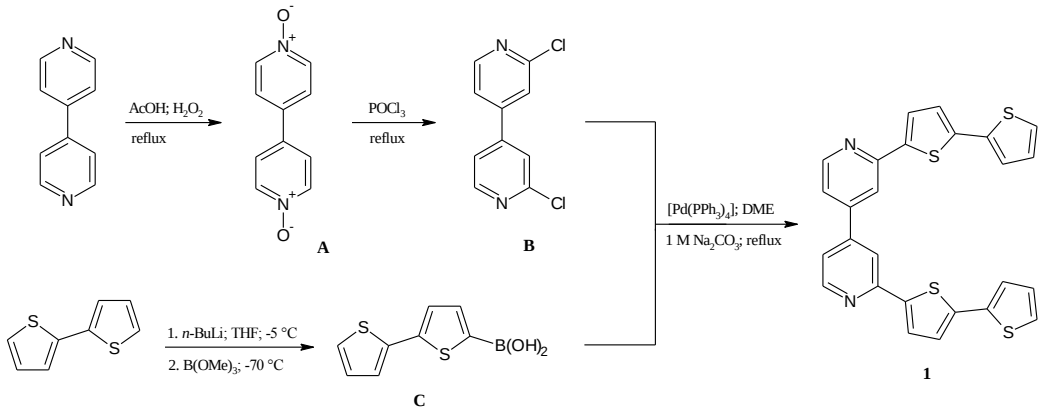

Scheme 2. Synthesis of 2,2'-bis(2,2'-bithiophen-5-yl)-4,4'-bipyridine (**1**).

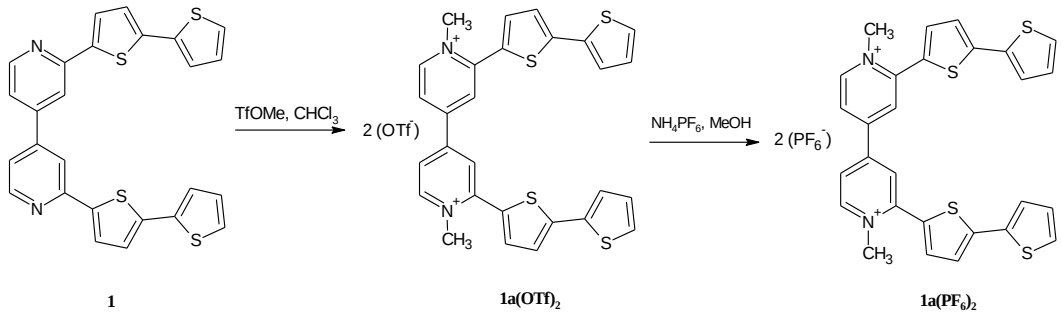

1 **1a(OTf)$_2$** **1a(PF$_6$)$_2$**

Scheme 3. Synthesis of methylviologenditriflate **1a(OTf)$_2$** and bis(hexafluorophosphate) **1a(PF$_6$)$_2$** salts.

Figures

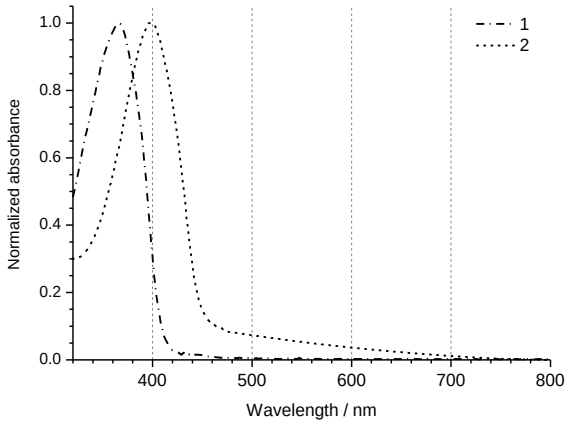

Fig. 1. UV-Vis absorption spectra of **1** and **2** recorded in dichloromethane solutions.

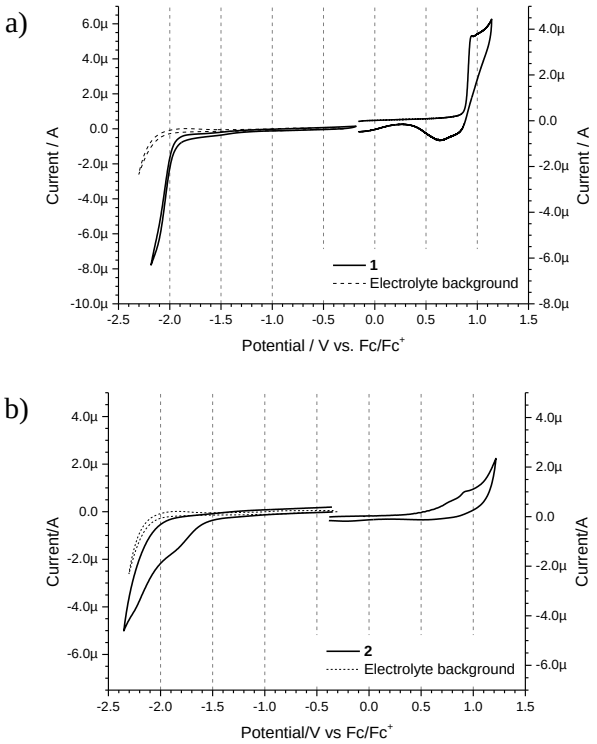

Fig. 2. Cyclic voltammograms of: a) 1.0 mM solution of **1**, b) saturated solution of **2**, in 0.1 M Bu_4NPF_6 in dichloromethane at platinum electrode. 100 mV/s sweep rate.

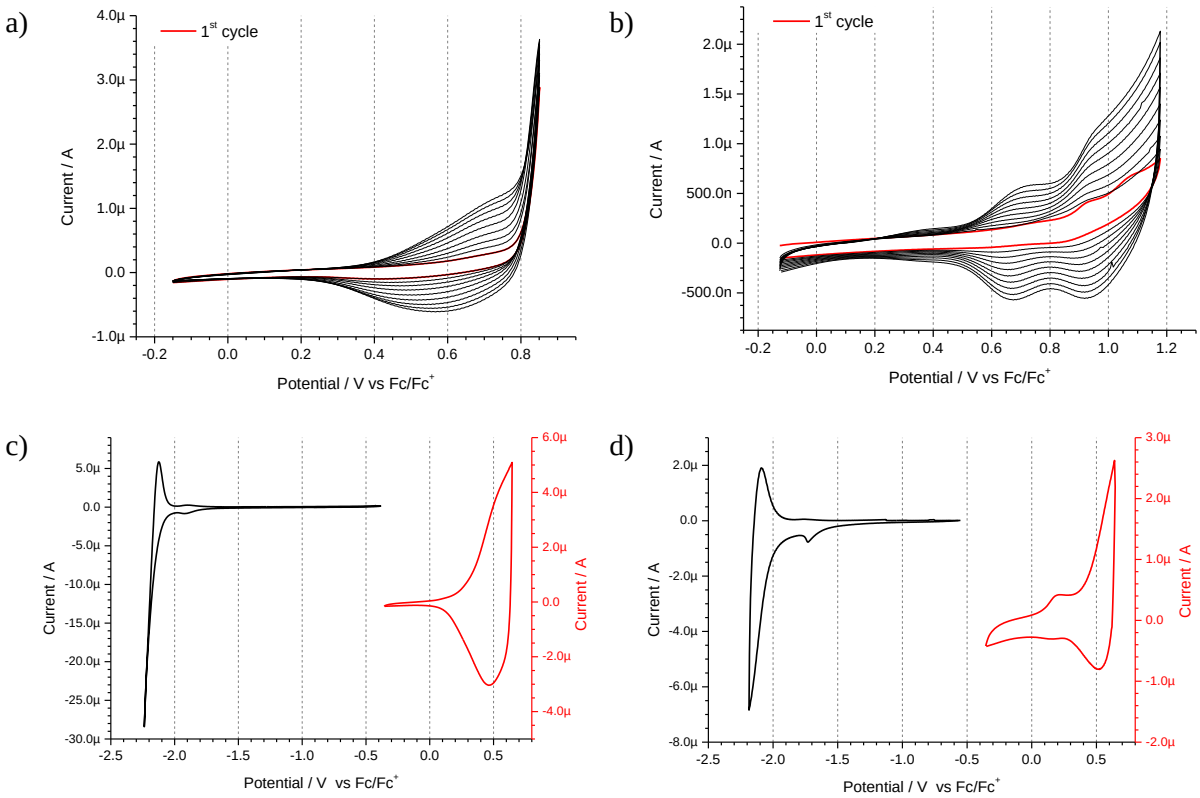

Fig. 3. Cyclic anodic oxidation of: a) 1.0 mM solution of **1**; b) saturated solution of **2**, in 0.1M Bu_4NPF_6 in dichloromethane, affording conductive polymer deposits at the platinum electrode. Individual anodic and cathodic cyclic voltammograms of deposition products: c) **p1**, d) **p2** in Bu_4NPF_6 in dichloromethane. Sweep rate: 100 mV/s for all measurements.

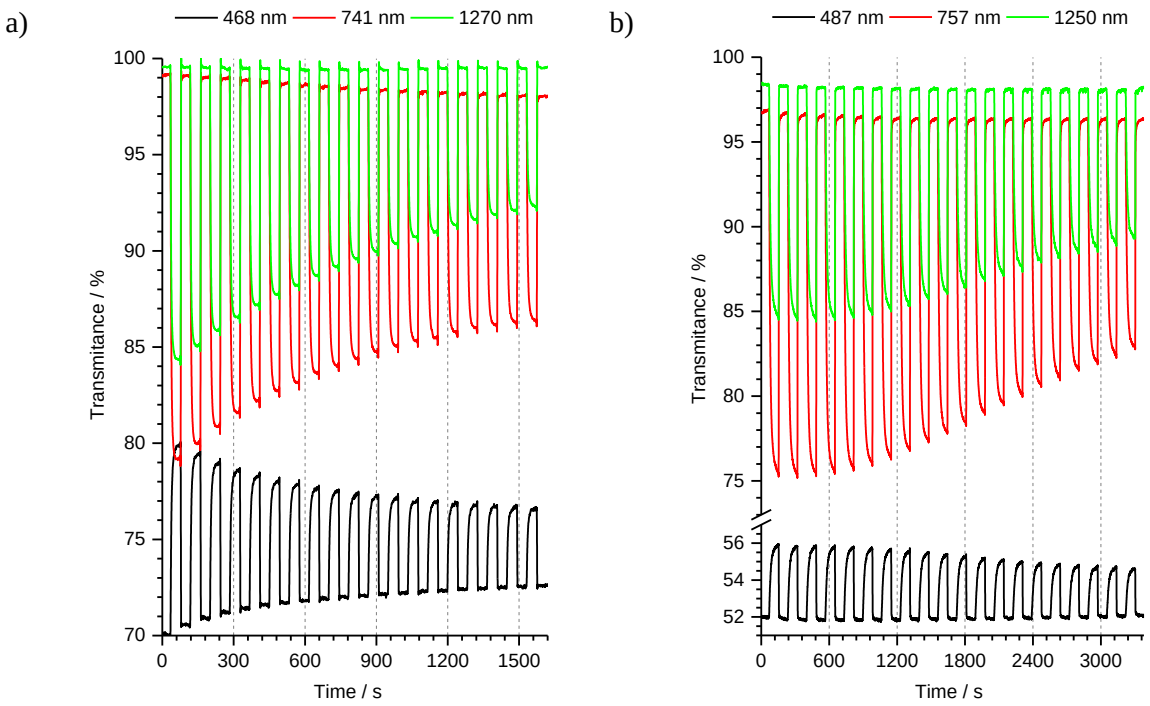

Fig. 4. Electrochromic switching response of: a) **p1** and b) **p2** polymer film during its p-doping/dedoping cycling. Step potentials: -0.4V and 0.65V; step duration for: **p1**: 40s, **p2**: 80s.

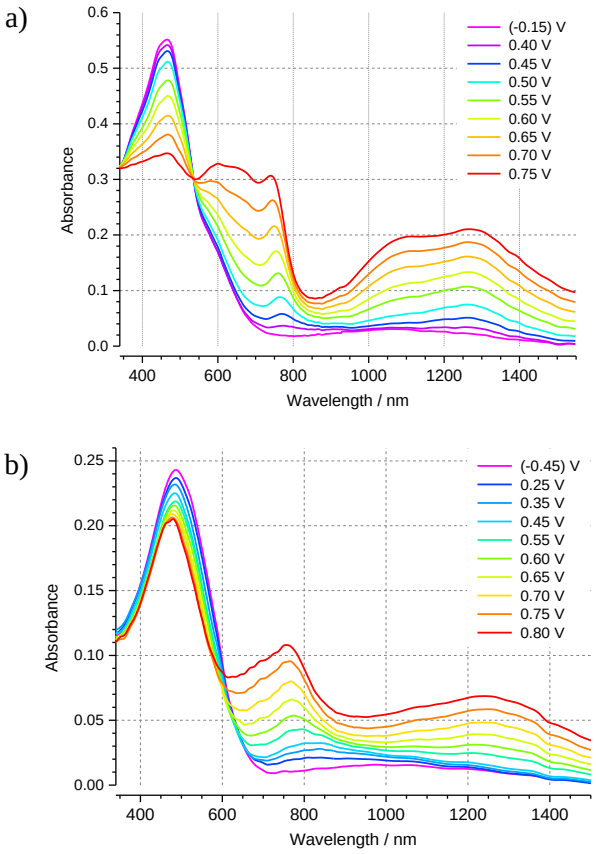

Fig. 5. UV-Vis-NIR spectra of potentiostatic anodic doping process of: a) **p1** and b) **p2** films, recorded during EPR/UV-Vis-NIR spectroelectrochemical experiments in 0.1M Bu_4NPF_6 in dichloromethane. Potentials given relative to Fc/Fc^+ reference.

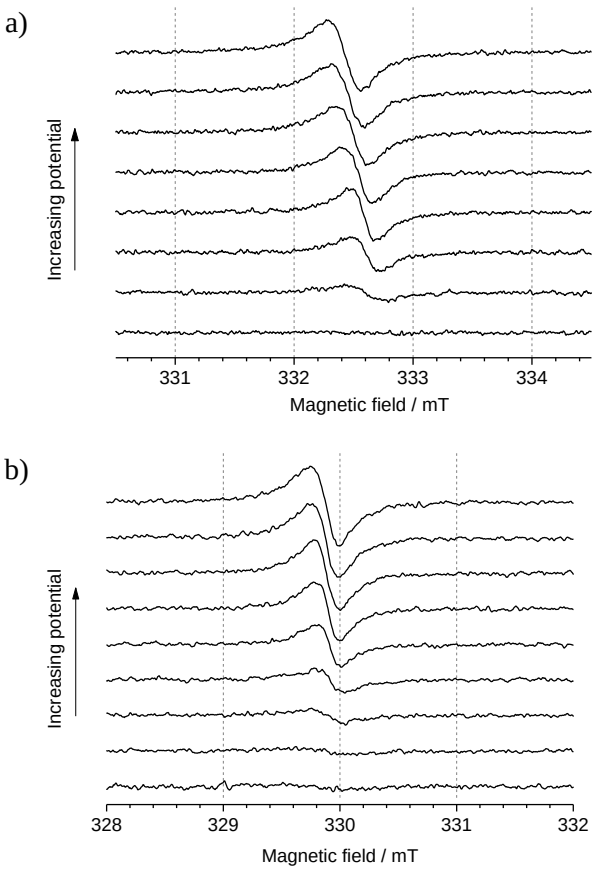

Fig. 6. Representative EPR spectra of: a) **p1** and b) **p2** registered during EPR/UV-Vis-NIR spectroelectrochemical experiments.

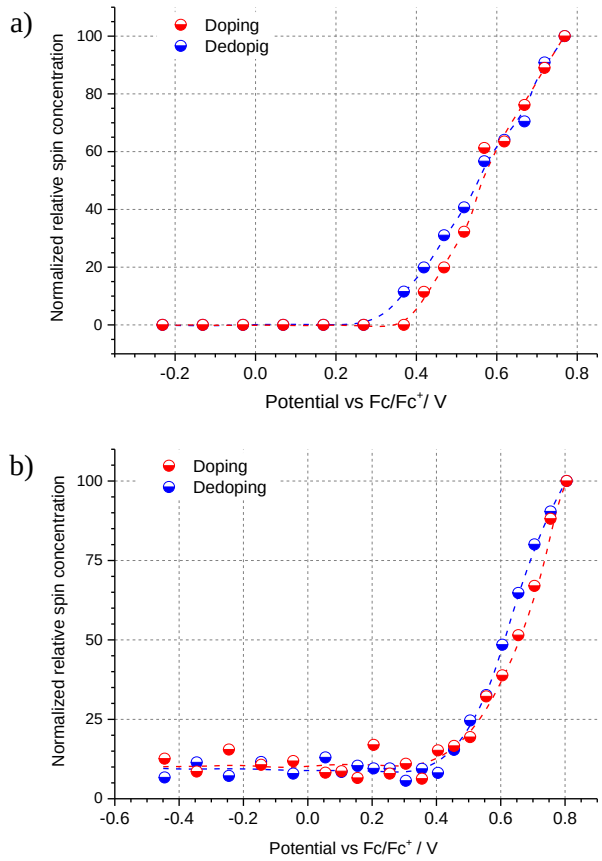

Fig. 7. Normalized relative spin concentration of: a) **p1** and b) **p2** as a function of applied potential during EPR/UV-Vis-NIR spectroelectrochemical experiments.

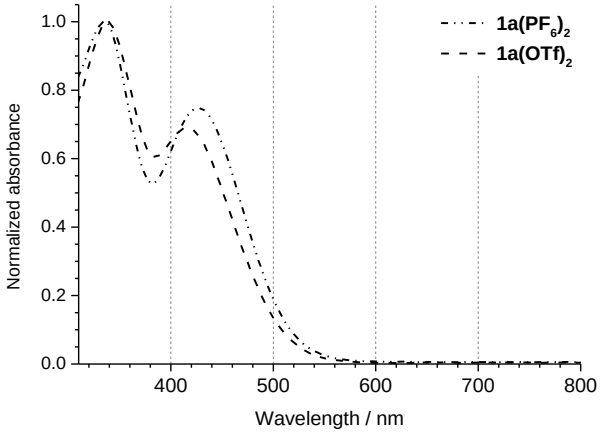

Fig. 8. UV-Vis absorption spectra of **1a(PF$_6$)$_2$** and **1a(OTf)$_2$** taken in dilute acetonitrile solutions.

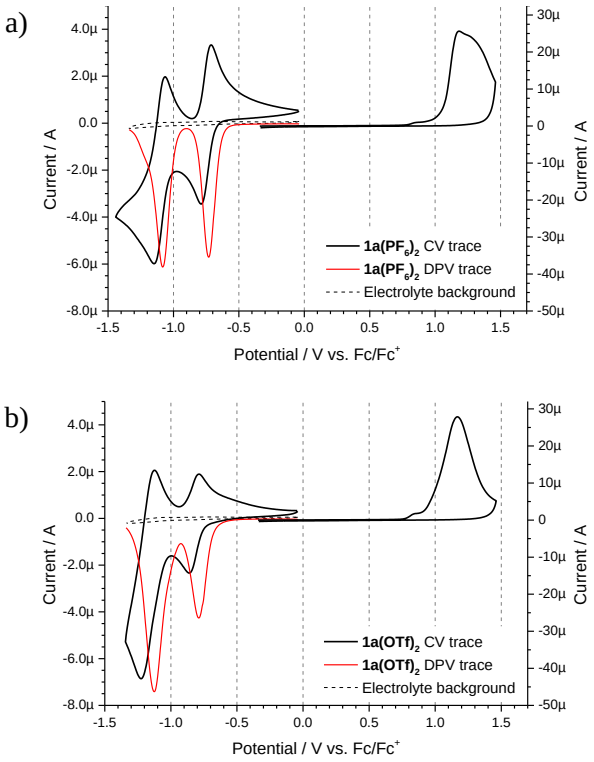

Fig. 9. Electrochemistry of 2mM solutions of: a) **1a(PF$_6$)$_2$** in 0.1M Bu_4NPF_6 in acetonitrile, and b) **1a(OTf)$_2$** in 0.1M Bu_4NOTf in acetonitrile at platinum electrode. CV sweep rate: 100mV/s. DPV potential pulse waveform: modulation time: 0.05s, interval time: 0.1s, step potential: 0.005V, modulation amplitude: 0.07V.

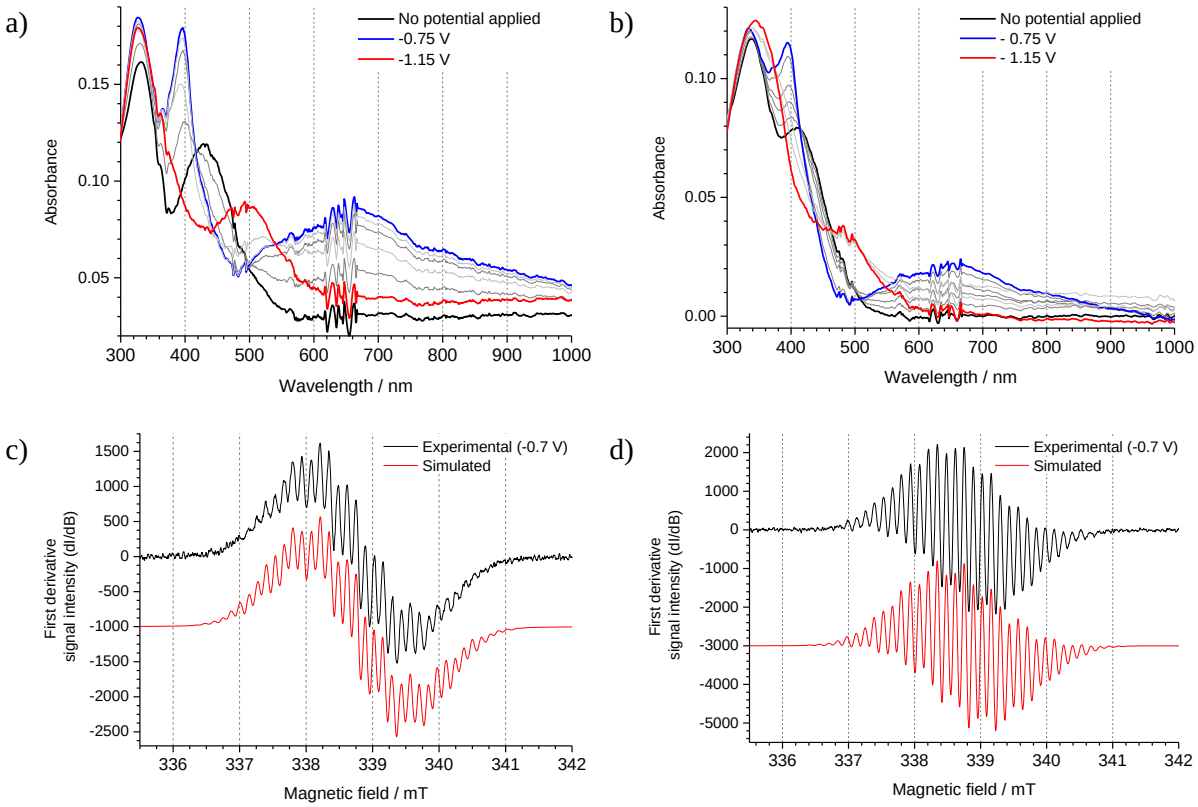

Fig. 10. Solution thin film UV-Vis-NIR spectroelectrochemistry of: a) **1a(PF$_6$)$_2$**, b) **1a(OTf)$_2$** and EPR spectroelectrochemistry of: c) **1a(PF$_6$)$_2$**, d) **1a(OTf)$_2$**. 1.0mM sample solution in 0.1M Bu_4NPF_6 (for a) and c)) or 0.1M Bu_4NOTf (for b) and d)) in acetonitrile. Spectra recorded in continuous electrolysis regime (potentials given on the respective plots). Hyperfine coupling constants and line parameters used for simulation of EPR spectra can be found in **Fig. S2** (Supporting Information).

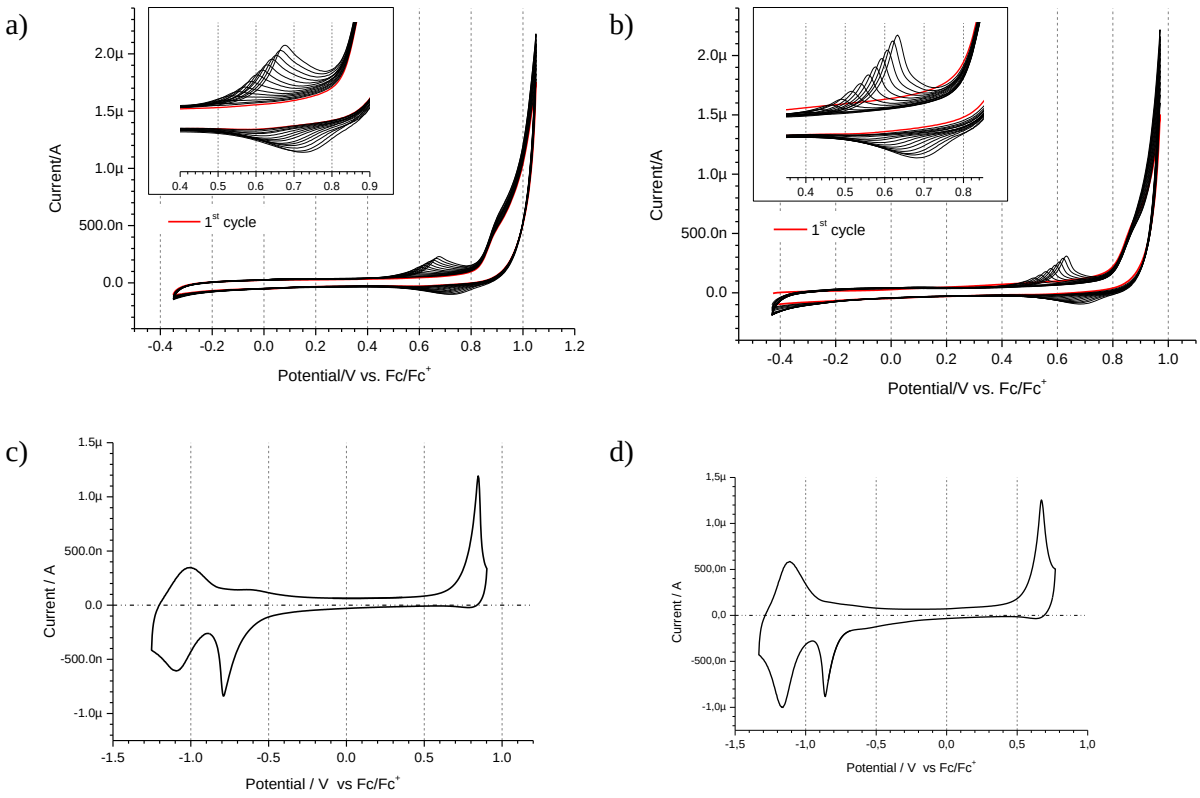

Fig. 11. Cyclic anodic oxidation of 1.0mM solutions of: a) **1a(PF$_6$)$_2$** in 0.1M Bu_4NPF_6; b) **1a(OTf)$_2$** in 0.1M Bu_4NOTf, in acetonitrile, affording polymer deposits at the platinum electrode. Cyclic voltammograms of deposition products: c) **p[1a(PF$_6$)$_2$]** in 0.1M Bu_4NPF_6; d) **p[1a(OTf)$_2$]** in 0.1M Bu_4NOTf, in acetonitrile. Sweep rate: 100 mV/s for all measurements.

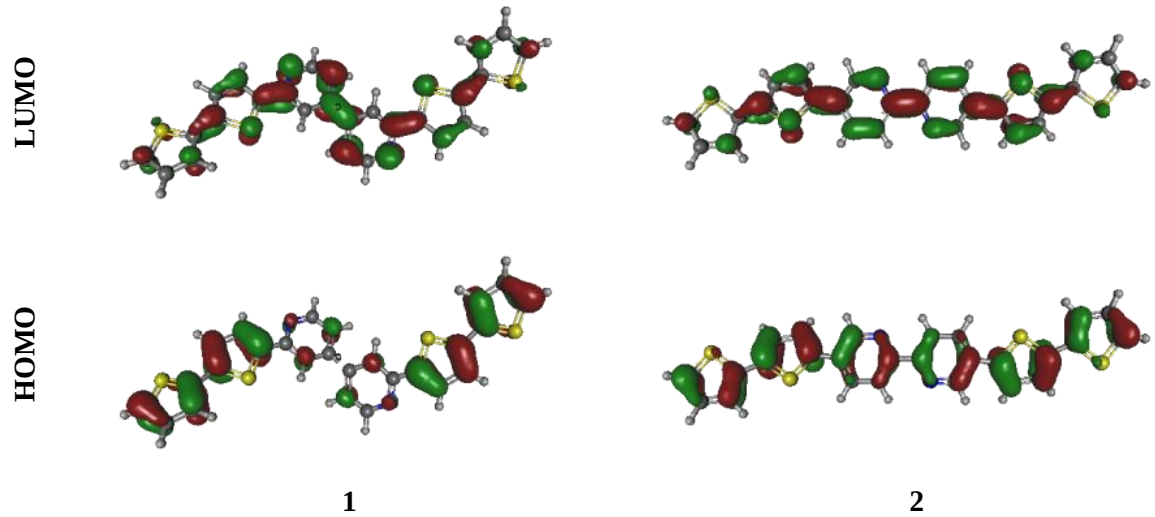

Fig. 12. Contours of frontier molecular orbitals of **1** and **2**, plotted at isovalue of 0.03 (green for positive and red for negative sign of wave function).

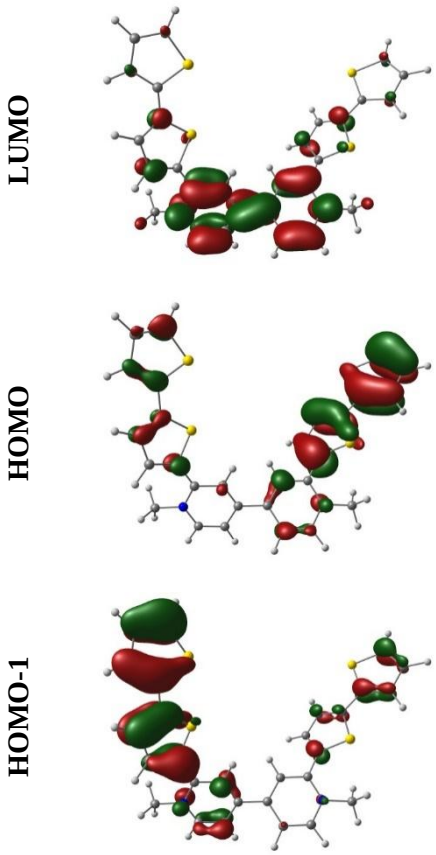

Fig. 13. Contours of frontier molecular orbitals of **1a**$^{2+}$plotted at isovalue of 0.03 (green for positive and red for negative sign of wave function).

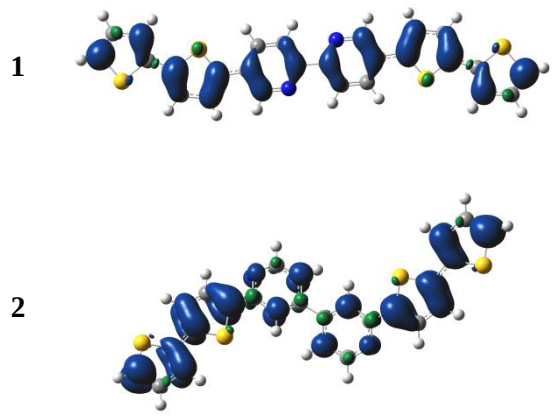

Fig. 14. Spin density plots for radical cations **1**$^{+\bullet}$ and **2**$^{+\bullet}$ at different geometries and at isovalue of 0.001 (blue for positive and green for negative values).

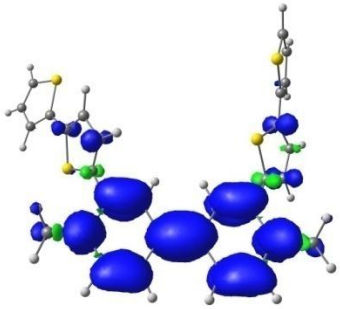

Fig. 15. Spin density plot for radical cation **1a**$^{+\bullet}$ at isovalue of 0.001 (blue for positive and green for negative values).

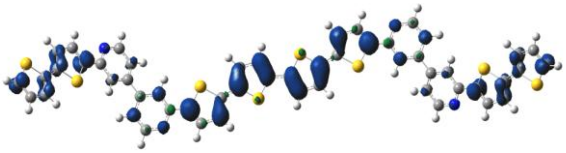

Fig. 16. Spin density plot for a $\mathbf{1}_2^{+\bullet}$ dimer at isovalue of 0.001 (blue for positive and green for negative sign of wavefunction).

Tables

Table 1 Spectroscopic and electrochemical data for discussed monomers **1** and **2**.

Compound	λ_{max} [nm]	E_g^{opt} * [eV]	$_{onset}E_1^{red}$ [V]	$_{onset}E_1^{ox}$ [V]	EA [eV]	IP [eV]	E_g^{ec} * [eV]
1	366	3.02	-1.96	0.88	3.14	5.98	2.84
2	399	2.79	-1.83	0.59	3.27	5.69	2.42

* Frontier molecular orbitals energy gap.

Table 2 Spectroscopic and electrochemical data for polymers with bipyridine units **p1** and **p2**.

Compound	λ_{max} [nm]	E_g^{opt} [eV]	$_{onset}E_1^{red}$ [V]	$_{onset}E_1^{ox}$ [V]	EA [eV]	IP [eV]	E_g^{ec} [eV]
p1	463	2.07	-2.11	0.27	2.99	5.37	2.38
p2	488	1.91	-2.01	0.06	3.09	5.16	2.07

Table 3 Electrochromic properties of **p1** and **p2** polymers.

Compound	λ^a [nm]	T_{dedop} [b] [%]	T_{dop} [c] [%]	ORT[d] [s]	$\lvert\Delta T\rvert$[e] [%]	Q_d[f] [$mC \cdot cm^{-2}$]	$\lvert CE\rvert$[g] [$cm^2 \cdot C^{-1}$]
p1	468	70.1	80.0	16.7	9.8	0.491	116
	741	99.2	79.2	11.1	20.0		199
	1270	99.5	84.4	11.4	15.1		146
p2	487	51.9	55.8	46.3	4.0	0.574	56
	757	96.8	75.6	38.2	21.2		187
	1250	98.5	84.9	40.7	13.6		112

[a] Analytic wavelength,
[b] Transmittance of dedoped polymer,
[c] Transmittance of doped polymer,
[d] Optical response time taken to reach 95% of maximum transmittance difference
[e] Electrochromic contrast,
[f] Doping charge density,
[g] Coloration Efficiency,
All parameters refer to the first doping switch of a pristine polymer film.

Table 4 Spectroscopic and electrochemical data for discussed monomers.

Compound	λ_{max} [nm]	E_g^{opt} * [eV]	E_1^{red} [V]	E_2^{red} [V]	$_{onset}E_1^{red}$ [V]	$_{onset}E_1^{ox}$ [V]	EA [eV]	IP [eV]	E_g^{ec} * [eV]
1a(PF$_6$)$_2$	338; 416	2.40	-0.75	-1.10	-0.69	0.79	4.41	5.89	1.48
1a(OTf)$_2$	336; 427	2.42	-0.82	-1.15	-0.75	0.77	4.35	5.87	1.52
2a(PF$_6$)$_2$ [a]	343; 262; 530	-	-0.66	-1.07	-0.58	0.89	4.44	5.99	1.76

* Frontier molecular orbitals energy gap.
[a] Data taken from reference [12].

Table 5 Electrochemical data for polymers with quaternised bipyridine units.

Compound	$_{onset}E_1^{red}$ [V]	$_{onset}E_1^{ox}$ [V]	EA [eV]	IP [eV]	E_g^{ec} [eV]
p[1a(PF$_6$)$_2$]	-0.60	060	4.50	5.70	1.20
p[1a(OTf)$_2$]	-0.71	0.55	4.39	5.65	1.26
p[2a(PF$_6$)$_2$] [a]	-0.12	0.40	4.98	5.50	0.52

[a] Taken from reference [12], polymer obtained with $BF_3{\cdot}Et_2O$ additive.